Supporting Information

for

A Dimeric Hydride-Bridged Complex with Geometrically Distinct Iron Centers Giving Rise to an $S = 3$ Ground State

Anne K. Hickey, Samuel M. Greer, Juan Valdez-Moreira, Sean A. Lutz, Maren Pink, Jordan A. DeGayner, T. David Harris, Stephen Hill, Joshua Telser, and Jeremy M. Smith*

Contents

Experimental

General Considerations. All manipulations were performed under a nitrogen atmosphere by standard Schlenk techniques or in an MBraun glove box. Glassware was dried at 140 °C overnight before cooling under a dynamic vacuum in an antechamber. Diethyl ether (Et_2O), tetrahydrofuran (THF), toluene, and pentane were purified by a Glass Contour solvent purification system. Celite was dried overnight at 130 °C under vacuum. The complex $Ph_2B(^tBuIm)_2FeCl(THF)$[1] was prepared by literature methods. Sodium triethylborohydride 1.0 M THF solution was purchased from Sigma-Aldrich and used as received. Deuterated solvents were purchased from Cambridge isotope labs. C_6D_6 and THF-d_8 were degassed and stored over molecular sieves for at least one day before use. All other chemicals were purchased and used as received. ^{1}H NMR spectroscopic data were recorded on Varian 400 MHz NMR spectrometers using J-Young tubes as sample holders. Solution magnetic susceptibilities were determined by Evans' method.[2] UV-Vis spectroscopic data were collected on an Agilent Technologies Cary 60 UV-Vis instrument. IR spectra were recorded with a Perkin Elmer spectrophotometer. Mössbauer spectra were recorded on a SEE Co spectrometer. The sample temperature was controlled using a SVT-400 Dewar from Janis equipped with a Lake Shore 255 Temperature Controller. The isomer shifts are reported relative to the centroid of the spectrum of α-Fe at 298 K. Samples were prepared by grinding crystallized material into a fine powder and then mounting in a cup, plugged with a fitted O-ring sealed cap. Data analysis was performed using the program WMOSS[3] and quadrupole doublets were fitted to Lorentzian lineshapes. Mass spectrometry measurements were made using an Agilent 1200 HPLC-6130 MSD spectrometer. Elemental analysis was conducted by Midwest Microlab, LLC (Indianapolis, IN).

Synthesis of $[Ph_2B(^tBuIm)_2FeH]_2$.

In a scintillation vial, $Ph_2B(^tBuIm)_2FeCl(THF)$ (537 mg 0.93 mmol) was dissolved in THF (3 mL). Sodium triethylborohydride solution (0.93 mmol, 0.93 mL of 1.0 M) was added slowly to the vial. A color change to dark blue occurred immediately upon addition of the borohydride solution. The mixture was then stirred for 3 h at room temperature, the solvent was removed under vacuum, yielding a black solid. The solid was washed with pentane (3 × 3 mL) to afford a dark blue solid (387 mg, 88% yield). Crystals suitable for X-ray diffraction were grown from a concentrated THF solution layered with pentane and stored at -35 °C overnight. ^{1}H NMR (THF-d_8, 400MHz) δ (ppm) 33, 18, 16, 7, 6, 2, 11, 19. Anal. Cald. for $C_{52}H_{66}B_2Fe_2N_8$: C 66.69, H 7.10, N 11.97; Found: C 66.67, H 7.31, N 11.64. The deuterated complex $[Ph_2B(^tBuIm)_2FeD]_2$ was prepared analogously using $NaBEt_3D$ solution.

The variable temperature ^{1}H NMR spectrum is consistent with a high symmetry species in solution, suggesting a fluxional, dimeric structure on the NMR timescale (Figure S1). The linearity of the Curie-Weiss plot is consistent with the presence of a single paramagnetic species in solution over this temperature range (Figure S2). Isosbestic points are observed in the VT UV-vis spectrum, suggesting the presence of an equilibrium that is slow on the UV-vis timescale (Figure S3). However, these data provide no structural information on the nature of the equilibrium.

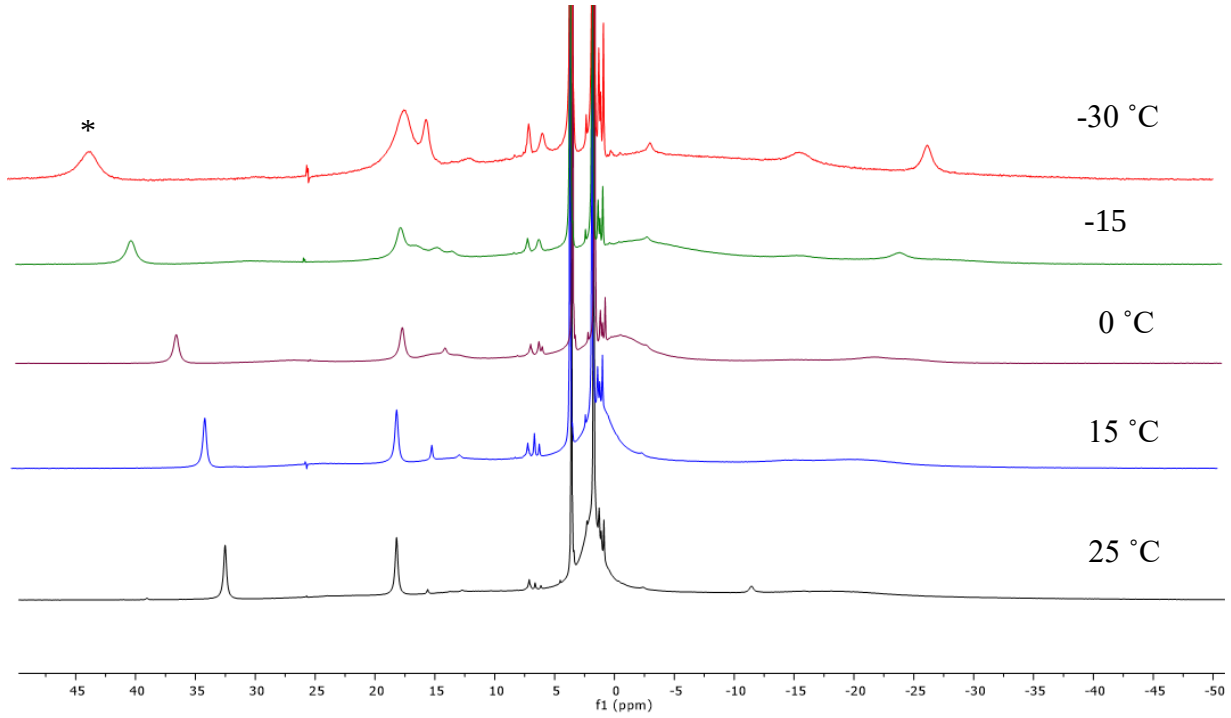

Figure S1. VT ^{1}H NMR spectra (400 MHz, THF-d_8) of $[Ph_2B(^{t}BuIm)_2FeH]_2$. The temperature dependence of the asterisked resonance was used to construct the Curie-Weiss plot in Figure S2.

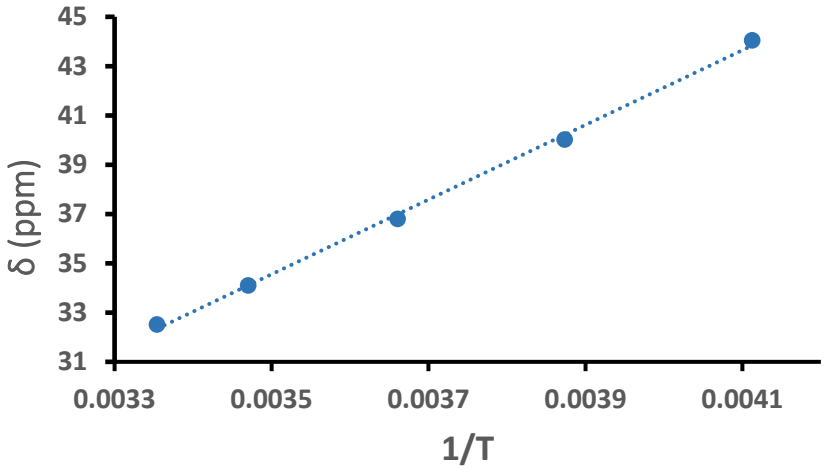

Figure S2. Curie-Weiss plot showing the linear relationship between chemical shift (ppm) and 1/T.

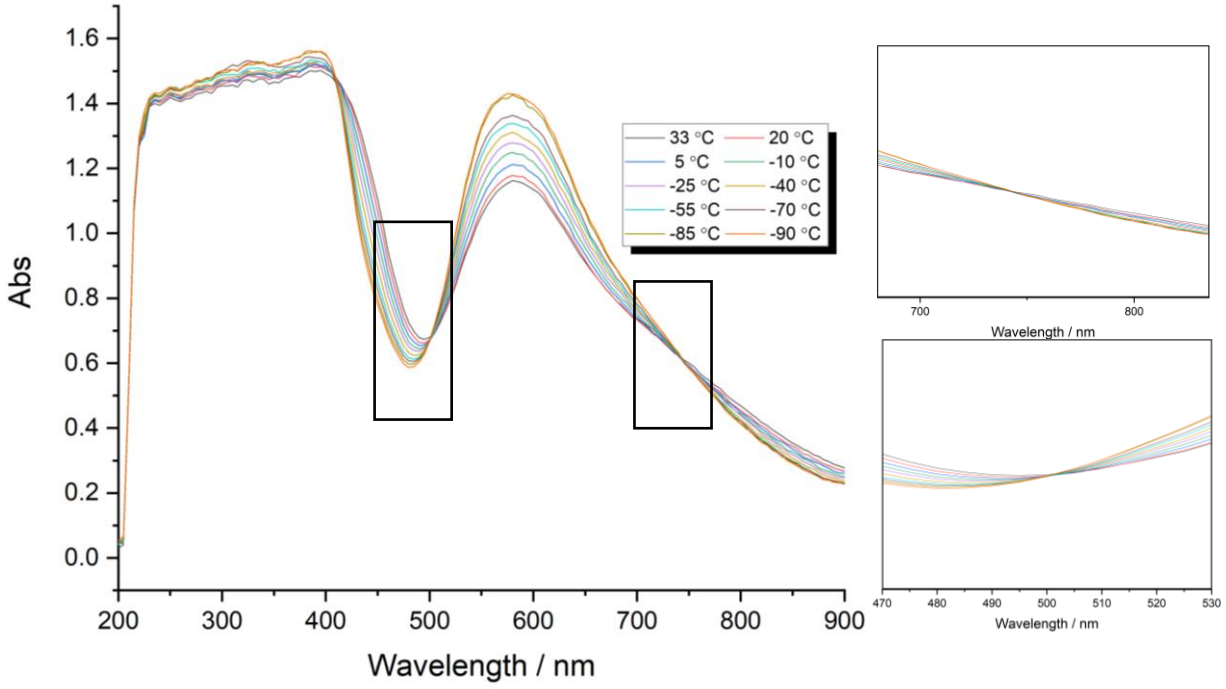

Figure S3. Variable-temperature UV-Vis spectra of $[Ph_2B(^tBuIm)_2FeH]_2$ in THF, between 33 and -90 °C. Two isosbestic points are observed at 501 and 744 nm.

Mössbauer Spectroscopy

The Mössbauer spectrum of $[Ph_2B(^tBuIm)_2FeH]_2$ can also be fit to two different subspectra, with δ = –0.0432 mm/s, ΔE_Q = 2.993 mm/s (60 %), and δ = +0.881 mm/s, ΔE_Q = 2.672 mm/s (40 %) (Figure S4). This alternative fit gives isomer shift and quadrupole splitting values that are not reasonable, in light of Mössbauer parameters reported for related complexes (Tables S1-S7).

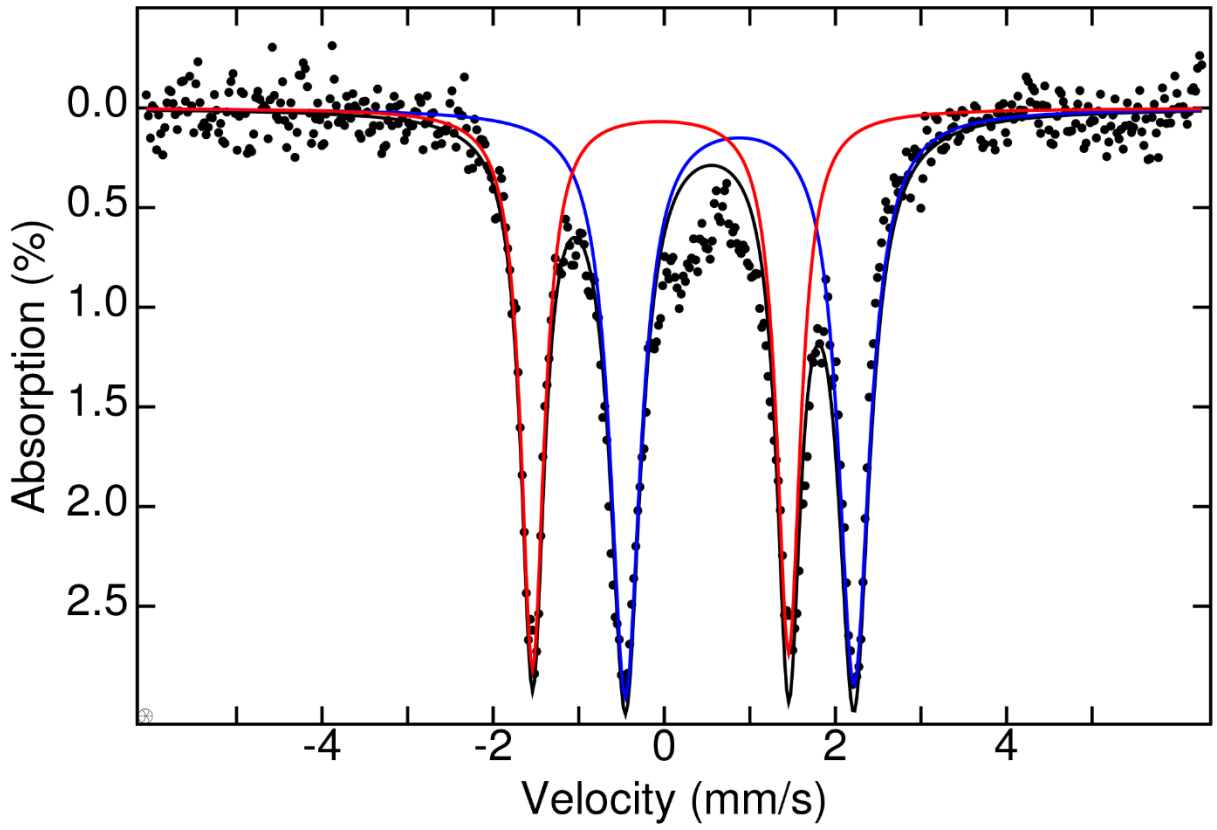

Figure S4. Solid state Mössbauer spectrum of $[Ph_2B(^tBuIm)_2FeH]_2$ at 80 K. Black circles represent experimental data, while red and blue lines correspond to fits of the spectral data that is an alternative to that shown in Figure 2 (main text), as described in the text.

Table S1. Mössbauer Spectral Parameters for Mononuclear Organometallic Fe(II) Complexes ($S = 2$) in a Tetrahedral Environment

Complex	δ (mm/s)	ΔE_Q (mm/s)	T (K)	Ref
$Fe(depe)Mes_2$	0.39	1.71	80	4
$Fe(IEt_2Me_2)_2Ph_2$	0.47	2.38	80	5
$Fe(IEt_2Me_2)_2$ (p-^{t}BuPh)$_2$	0.45	2.4		5
$Fe(IEt_2Me_2)_2(CH_2SiMe_3)_2$	0.49	2.53		5

depe = 1,2-bis(diethylphosphino)ethane

IEt_2Me_2 = 1,3-diethyl-4,5-dmethylimidazol-2-ylidene

Table S2. Mössbauer Spectral Parameters for Mononuclear Organometallic Fe(II) Complexes ($S = 1$) in a Square Planar Environment.

Complex	δ (mm/s)	ΔE_Q (mm/s)	T (K)	Ref
$Fe(PEt_2Ph)_2Mes_2$	0.31	4.63	80	4
$Fe(dppe)Mes_2$	0.33	4.53		4
$Fe(C_6Cl_5)_2(PEt_3)_2$	0.29	4.16	79	6
$Fe(C_6Cl_5)_2(PEt_2Ph)_2$	0.25	4.13		6
$Fe(IEt_2Me_2)_2((3,5\text{-}CF_3)_2C_6H_3)_2$	0.17	4.09	80	5

dppp = 1,2-bis(diphenylphosphino)ethane)

IEt_2Me_2 = 1,3-diethyl-4,5-dmethylimidazol-2-ylidene

Table S3. Mössbauer Spectral Parameters for Mononuclear Fe(II) Complexes ($S = 2$) in a Square Planar Environment.

Complex	δ (mm/s)	ΔE_Q (mm/s)	T (K)	Ref
$[Na_2(Et_2O)_4][Fe_2(^tBuSi(OSiMe_2O)_2)_2]$	0.91	0.37	80	7
$[CF_3\text{-}ONO]FeClLi_2(Et_2O)_2$	0.83	0.45	4.2	8

$Fe_2(^tBuSi(OSiMe_2O)_2)_2$ =

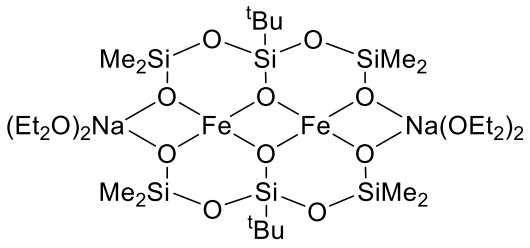

CF_3-ONO =

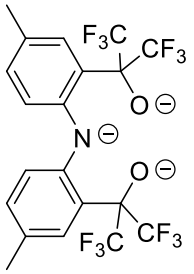

Table S4. Mössbauer Spectral Parameters for Mononuclear Fe(I) Complexes (S = 1/2) in a Square Planar Environment.

Complex	δ (mm/s)	ΔE_Q (mm/s)	T (K)	Ref
$Fe(I^iPr_2Me_2)_4^+$	0.36	1.92	200[a]	9
$Fe(TPP)^-$	0.65	2.23	77	10
$L^{xyl}Fe(CO)_2$	0.18	2.04	80	11

[a] – Spectrum is heavily broadened at 80 K due to slow paramagnetic relaxation.

TPP = tetraphenylporphyrin dianion

$I^iPr_2Me_2$ = 1,3-bis(isopropyl) -4,5-dmethylimidazol-2-ylidene

L^{xyl} = 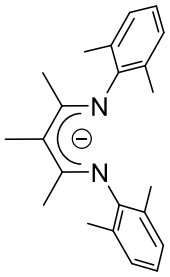

Table S5. Mössbauer Spectral Parameters for Mononuclear Fe(I) Complexes (S = 3/2) in a Tetrahedral Environment.

Complex	δ (mm/s)	ΔE_Q (mm/s)	T (K)	Ref
$L^{Me}Fe(^tBupy)_2$	0.79	0.59	80	12
$Fe(IMe_2Me_2)_4^+$	0.57	0.17	80	9
$Fe(IEt_2Me_2)_4^+$	0.57	0.82		9

L^{Me} =

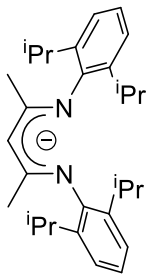

IMe_2Me_2 = 1,3,4,5-tetramethylimidazol-2-ylidene

IEt_2Me_2 = 1,3-diethyl-4,5-dmethylimidazol-2-ylidene

Table S6. Mössbauer Spectral Parameters for Mononuclear Fe(III) Complexes.

Complex	δ (mm/s)	ΔE_Q (mm/s)	T (K)	Ref
Square Planar (S = 3/2)				
$Fe(qdt)_2$	0.23	3.7	80	13
$Fe(TipsiPP)^+$	0.33	5.16	6	14
Tetrahedral (S = 1/2)				
$L^{Me}FeCl_2$	0.29	1.79	80	15

qdt = *o*-quinoxalinedithiolato.

TipsiPP = 5,10,15,20-tetrakis(2',6'-bis(triisopropylsiloxy)phenyl)porphyrin dianion.

L^{Me} = 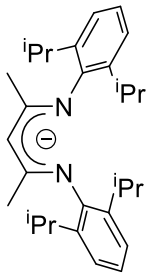

Table S7. Mössbauer Spectral Parameters for β-Diketiminate Fe_2H_2 and Fe_2D_2 Complexes.

Complex	δ (mm/s)	ΔE_Q (mm/s)	T (K)	Ref.
$[L^{Me}FeH]_2$	0.51	2.05	80	16
$[L^{Me}FeD]_2$	0.51	2.10		16
$[L^{tBu}FeH]_2$	0.59	1.58	80	17
$[L^{tBu}FeD]_2$	0.58	1.74	80	16
$[L^{Me,Et}FeH]_2$	0.66	1.27	80	18

L^{Me} =

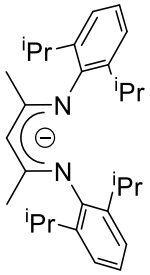

L^{tBu} =

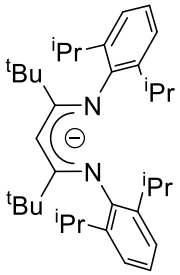

$L^{Me,Et}$ =

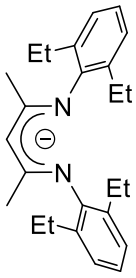

Magnetic Measurements

Magnetic measurements of $[Ph_2B(^tBuIm)_2FeH]_2$ were performed on polycrystalline samples restrained with eicosane wax and flame-sealed in a quartz tube under vacuum. All data were collected using a Quantum Design MPMS-XL SQUID magnetometer from 1.8 to 300 K at applied dc fields ranging from 0 to +7 T. Dc susceptibility data were corrected for diamagnetic contributions from the eicosane wax and from the core diamagnetism of the sample (estimated using Pascal's constants[19]).

Electronic Absorption Spectra of $[Ph_2B(^tBuIm)_2FeH]_2$.

The electronic absorption spectrum of $[Ph_2B(^tBuIm)_2FeH]_2$ is not especially rich, but does exhibit bands that are informative and consistent with the assignment to two Fe(II) ions, one being tetrahedral, high-spin ($S = 2$) and the other square planar, intermediate-spin ($S = 1$). The UV-Vis-NIR spectrum recorded in C_6D_6 (to mitigate C-H overtone vibrational bands in the NIR) is shown in Figure S5. There are strong bands below 500 nm, in particular one that is resolved at 356 nm (ε = 7000 L mol^{-1} cm^{-1}). These are attributed to ligand-to-metal-charge transfer (LMCT) bands, based on analogous complexes of both imidazolylidene (NHC) and pyrazolyl chelating ligands.[20] Further into the UV region are bands that were not investigated, but are due to intra-ligand transitions. Of interest are the two bands in the Vis-NIR region: one at 585 nm (17 080 cm^{-1}; ε =1100 L mol^{-1} cm^{-1}, although the tail of the CT bands likely contribute to its intensity) and a weak one at roughly 1190 nm (8400 cm^{-1}; $\varepsilon \approx 150$ L mol^{-1} cm^{-1}). The first can be assigned to a d-d transition of the square planar Fe(II) ion and the latter either wholly or partly to a transition of the tetrahedral Fe(II) ion, in particular by analogy with four-coordinate organometallic Fe(II) complexes[5] of general type FeL_2R_2, where L = mono- or bidentate (i.e., $Fe(LL)R_2$) NHC ligands and R = aryl or alkyl moieties. For example, two tetrahedral complexes reported by Deng and co-workers, where LL = bidentate-NHC and R = aryl, exhibit broad NIR bands at 1330 (7520 cm^{-1}) and 1410 nm (7090 cm^{-1}).[21] This is because tetrahedral Fe(II) complexes exhibit a weak band in the NIR region due to the transition $^5E \rightarrow {}^5T_2$ (T_d point group symmetry;[22] e.g., at 4800 cm^{-1} for $[FeCl_4]^{2-}$ in a chloride melt).[23] The ligand field of hydrocarbyl, hydride, and imidazolyl (NHC) donors is expected to be stronger than that of chloride ions, blue-shifting the transition as seen here and in previous cases.[5,21] In addition, the symmetry of the tetrahedral site in these cases is more accurately given as only C_{2v}. We have used a simple ligand-field theory (LFT) angular overlap

model (AOM) to describe this transition. Use of the actual bond angles with idealized four-fold symmetry (C donors at $\theta = 46.54^{o}$, H donors at 141.85^{o}, and $\phi = 0, 180^{o}, 90^{o}, 270^{o}$ for these in order) with AOM bonding parameters: $\varepsilon_{\sigma}(C) = 8017\ cm^{-1}$, $\varepsilon_{\sigma}(H) = 5933\ cm^{-1}$, and interelectronic repulsion (Racah) parameters: $B = 700\ cm^{-1}$ (reduced to ~80% of the Fe^{2+} free-ion value)[24] $C = 3100\ cm^{-1}$ ($C/B = 4.43$, versus 4.32 in free-ion Fe^{2+}).[24] There is obviously no π-bonding for the hydrido ligands and for simplicity, we ignore π-bonding for the imidazolylidenes. Previous studies suggest that π-bonding, whether donating or accepting, is small for this ligand type.[25] The sole reference point of which we are aware for a hydrido ligand in our context is the interesting homoleptic, low-spin ($^{1}A_{1g}$ ground state in O_h) complex $[FeH_6]^{4-}$.[26-28] The countercations are four $[MgX(THF)_2]^{+}$, where X = Cl or Br, or a mixture of the two. The crystal structures of $[FeH_6]^{4-}$ (CSD codes: BASLIQ, BASLIQ01, BASLIQ10) using both x-ray[27,28] and neutron[28] diffraction show direct interaction between the Mg(II) ions and hydrido ligands to Fe(II), forming a $[Mg_4FeH_6]^{4+}$ unit with the Mg(II) ions at the corners and the hydrides at the faces of a Fe(II)-centered cube.[27,28] A thorough investigation by Linn and Gibbins of the electronic absorption spectra of this complex in THF solution yielded $\varepsilon_{\sigma}(H) = 8250\ cm^{-1}$ (based on the midpoint of their range of Δ_{H^-} values).[26] A hydrido ligand bridging between two Fe(II) ions would be expected to be a weaker donor than one bridging Mg(II) and Fe(II) ions since the interaction with Mg(II) is less covalent than with Fe(II) (some association of Mg(II) ions with the $[FeH_6]^{4-}$ unit persists in THF solution),[26] so the estimate made here for $\varepsilon_{\sigma}(H)$ seems reasonable.

The situation with respect to the square planar site is even more challenging because of the dearth of truly analogous Fe(II) complexes (i.e., those lacking any axial ligands *and* without forced planar geometry). Many examples of macrocyclic (often tetrapyrroles)[29] Fe(II) complexes with such enforced square planar tetra-coordination are known. A rare example of the corresponding square

planar Fe(III) with no axial ligands is that reported by Suslick and co-workers,[14] $[Fe^{III}(TipsiPP)]^+$, where H_2TipsiPP is 5,10,15,20-tetrakis(2′,6′-bis(triisopropylsiloxy)phenyl)-porphyrin, an extremely sterically hindered porphyrin. This $3d^5$ complex exhibits an $S = 3/2$ ground state, which is analogous to the $S = 1$ ground state proposed for the planar site in $[Ph_2B(^tBuIm)_2FeH]_2$. Moreover, the electronic absorption spectra of most such complexes are dominated by ligand-centered bands. There are also square planar complexes of Fe(II) with the appropriate geometry, such as the pincer complexes reported by Pascualini et al.,[8,30] but these have $S = 2$ ground states, so that the spin-allowed electronic transitions are quite different. To apply the AOM, we treat this Fe(II) site as ideally planar, with the *z*-axis defined as normal to the molecular plane, to be consistent with a truly square (D_{4h}) complex; thus, $\theta = 90^o$ for all four ligands. We define the *x*-axis as along the Fe-Fe vector; the ∠H-Fe-H is 84.89° and ∠C-Fe-C is 87.14°, so we set $\phi = 42.44^o$ and 317.56° for the hydrido ligands, and 136.43° and 223.57° for the NHC donors. If the same Racah and bonding parameters are used as for the tetrahedral site (the latter rounded to $\varepsilon_\sigma(C) = 8000$ cm^{-1}, $\varepsilon_\sigma(H) = 5900$ cm^{-1}), then the ground state is indeed a spin triplet with triplet excited states located at 14 200 – 15 600 cm^{-1} and at 19 100 – 20 000 cm^{-1} above the ground state. Spin-allowed transitions to any among these could correspond roughly to the observed Vis band. To obtain a closer match, any of the relevant parameters ($\varepsilon_\sigma(H)$, $\varepsilon_\sigma(C)$, *B*, or *C*) could be modified, which is an unreasonably large parameter space given the limited experimental data. Solely as an illustration, however, we allow $\varepsilon_\sigma(C)$ to vary, the justification being that the μ-hydrido ligands bond equally to the two Fe(II) ions, and that the Racah parameters would be essentially the same for Fe(II) ions with the same donor set. An exact match to the observed band for the lowest of the above higher set of triplet states then obtains with $\varepsilon_\sigma(C) = 6546.4$ cm^{-1}, with the other parameters unchanged from the values used previously.

This choice of LFT parameters affords a triplet ground state with very low-lying quintet and singlet excited states. Their relative energies could be adjusted by changing the Racah parameters, although this ability is limited because an increase in the Racah parameters could make the ground state a singlet and a decrease would favor the quintet. The ground state can be described in strong field notation as $d_{x^2-y^2}{}^2 d_{xz}{}^2 d_{yz}{}^1 d_{z^2}{}^1 d_{xy}{}^0$. Note that because the *x*-axis is defined between the bonds (along the Fe-Fe vector), d_{xy} makes up the Fe-L σ* MO, rather than $d_{x^2-y^2}$. The modest deviation from four-fold symmetry leads to the d_{xz} orbital being slightly lower in energy than d_{yz}. Using the C_{2v} point group with C_2 defined along *x* rather than *z*, which we have done previously,[31] means that this ground state is $^3A_2$ rather than $^3B_2$. There are a number of triplet excited state; however, the lowest lying are too close in energy to the ground state (~3900 – 6400 cm^{-1}) to be observable by optical spectroscopy and the next range, while in the NIR region (~11 400 – 14 000 cm^{-1}), involve multi-electron transitions, although these may contribute to the shoulder seen experimentally at ~800 nm (~12 500 cm^{-1}). The next range of triplet excited states (~17 080 – 17 800 cm^{-1}), however, likely corresponds to the observed Vis transition as it includes dipole-allowed single-electron transitions. A complete listing of the electronic states of this AOM generated using the program Ligfield[32] is given in Table S11.

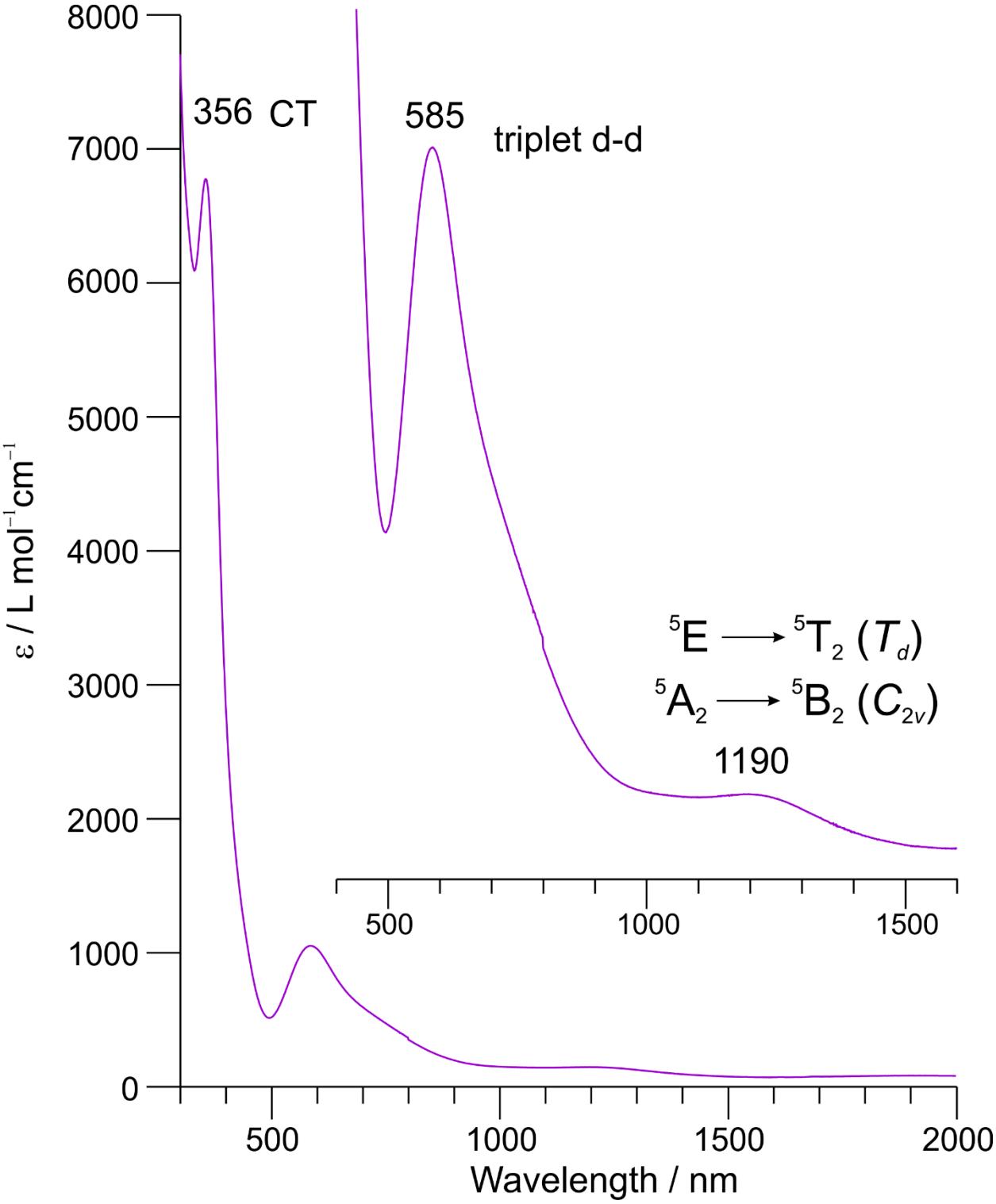

Figure S5. UV-Vis-NIR spectrum of $[Ph_2B(^tBuIm)_2FeH]_2$ in C_6D_6 solution. See text for discussion on band assignments.

HFEPR Spectroscopy

High frequency and -field EPR (HFEPR) measurements were performed on a constrained powder sample of $[Ph_2B(^tBuIm)_2FeH]_2$. The series of frequency-dependent spectra recorded in the range of 208 – 634 GHz at both 5 K and 20 K are shown in Figures S6a and S6b, respectively. The spectra recorded at 5 K and below 600 GHz are dominated by lines which correspond to molecular oxygen and are marked by asterisks in Figure S6. We also observe a very weak feature (indicated by #) near $g = 2.00$ which originates from the presence of a minor radical contaminant. The final feature occurs at $g \sim 14$ (pink circle) and could arise from transitions within the $m_S = \pm 3$ quasi-doublet. Such a transition would require that D is negative, $E \neq 0$, and that $g_z \approx 2.3$. The narrow linewidth of this transition is unusual and seems inconsistent with the broad lines observed at higher frequencies (vide infra) but the large g-value precludes any of the normally observed containments, e.g. molecular oxygen and radical-based impurities. Thus we can assign it as originating from the compound of interest. In spectra recorded at 5 K and above 600 GHz we observe a single transition which moves towards zero field as the frequency increases. Examining a pair of Zeeman diagrams (Figure S7) generated for both signs of D suggests that both cases could produce such a transition at low temperatures (orange circle in Figure S6). Upon raising the temperature to 20 K we observe three additional lines, described as follows. The first line intercepts zero field at ~208 GHz and increases in field position with increasing frequency (red circle). The second line is observed in the 610 and 634 GHz spectra and its resonance field increases with frequency (green circle). A third line is observed at moderate field values which moves toward lower fields as the frequency is increased (blue circle). We note that both axial cases ($D > 0$ and $D < 0$), which could describe the low temperature (5 K) behavior of the 610 and 634 GHz spectra, fail to reproduce any of these additional higher temperature (20 K) lines. Thus, we can deduce the

presence of a non-zero rhombic component to the anisotropy, i.e., $E \neq 0$. This is consistent with the assignment of the peak noted in pink (Figure S6). The HFEPR spectra were simulated using a standard $S = 3$ spin-Hamiltonian:

$$\hat{H}_{spin} = \beta_e \vec{\mathbf{B}} \cdot \tilde{\boldsymbol{g}} \cdot \hat{\boldsymbol{S}} + D\left[\hat{S}_z^2 - \frac{S(S+1)}{3} + \frac{E}{D}\left(\hat{S}_x^2 - \hat{S}_y^2\right)\right] + B_4^0 \hat{O}_4^0,$$

where β_e is the Bohr magneton, $\vec{\mathbf{B}}$ is the magnetic field vector, $\tilde{\boldsymbol{g}}$ is the g-tensor, D/E are the second order axial and rhombic zfs parameters, B_4^0 is the fourth order axial zero field splitting (defined by $\hat{O}_4^0$) parameter, $\hat{\boldsymbol{S}}$ is the total electronic spin operator, and $\hat{S}_\mu$ ($\mu = x, y, z$) its components. During our efforts to simulate the spectra, we noticed that the prominent transitions all seemed to occur with B_0 parallel to the z component of the anisotropy axis. Thus, we initially simulated the data using a single orientation. This procedure furnished the following set of parameters: $D = -7.1$ cm^{-1}, $|E| = 2.1$ cm^{-1} ($|E/D| = 0.30$), $B_4^0 = 0.0055$ cm^{-1}, and $g_z = 2.30$ (Figure S8). We then used these parameters to simulate the powder averaged spectrum which successfully reproduced essentially all the observed features. The values for g_x and g_y were then adjusted to reproduce the peaks which were missed with the initial parameterization and resulted in $g_x = 2.00$ and $g_y = 2.15$ (Figure S9). Efforts to reproduce the data without B_4^0 were significantly less promising and led to too large a difference in resonance position between the peaks noted in orange and green (Figure S6).

In addition to the $[Ph_2B(^tBuIm)_2FeH]_2$ compound, we have also studied an isotopolog wherein the bridging hydrides are replaced by deuterides. Given the sensitivity of EPR to changes in spin Hamiltonian parameters, we would expect any changes in structure and/or the exchange interaction as a result of H-to-D substitution to manifest in the EPR spectrum. Spectra of $[Ph_2B(^tBuIm)_2FeD]_2$ are reported in Figure S10. Comparison of the spectra of the deuterated and

protonated samples reveal no discernable changes in resonance positions. Thus, we find that no isotope effects exist in this μ-H_2 complex.

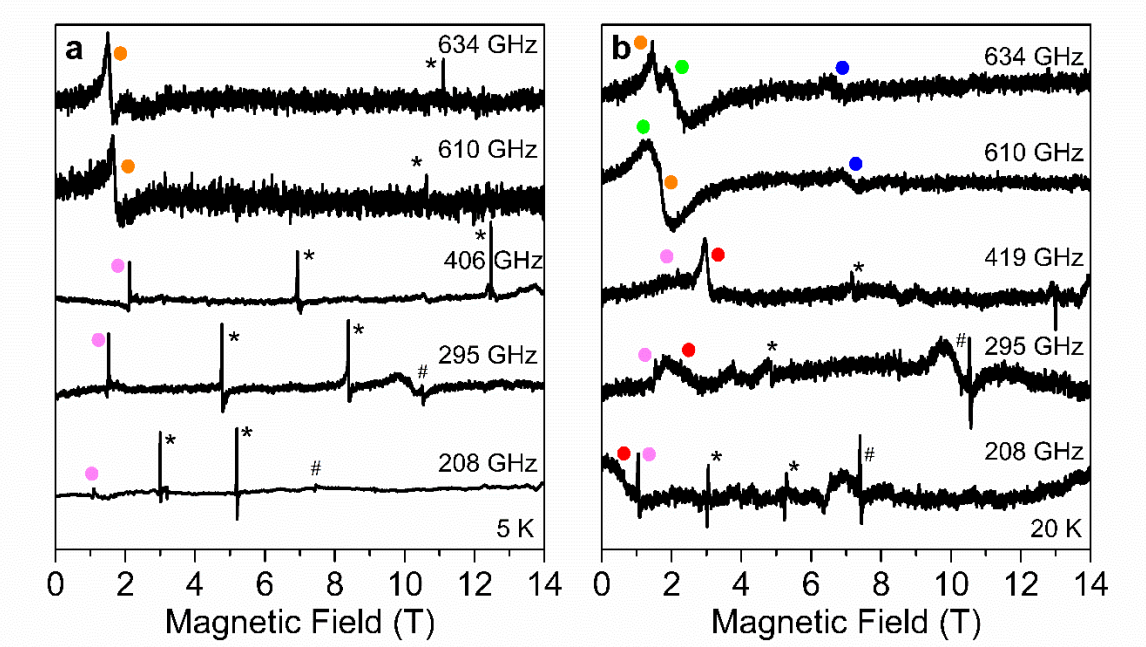

Figure S6: HFEPR spectra of a constrained sample of $[Ph_2B(^tBuIm)_2FeH]_2$ recorded at multiple frequencies at 5 K (a) and 20 K (b). The color markers are from the di-Fe(II) complex and are described in the accompanying text; asterisks indicate signals due to O_2(s); a minor radical impurity is denoted by #.

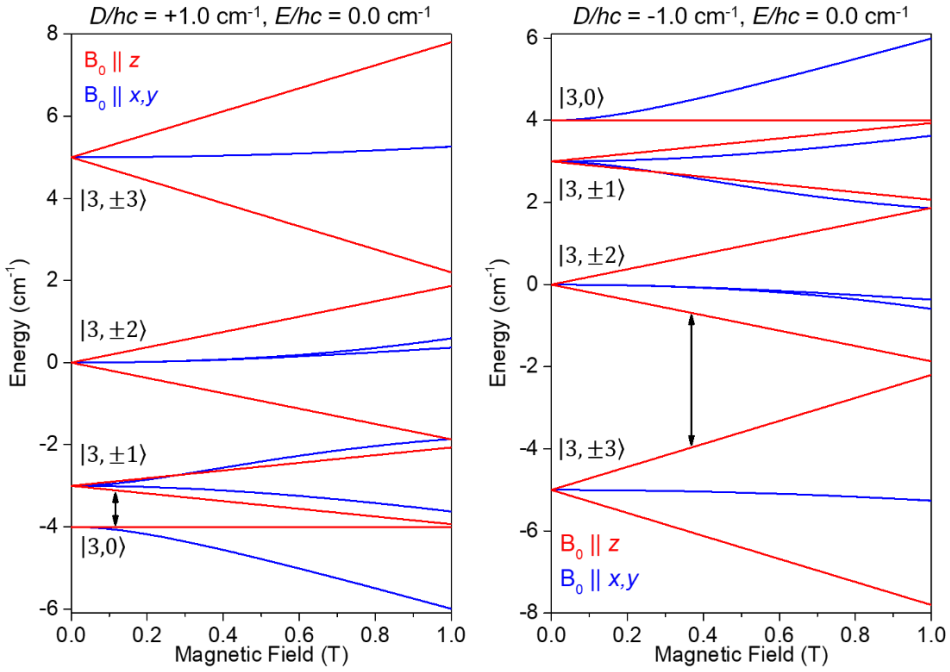

Figure S7: Zeeman diagrams of the two cases of axial zero field splitting: $D > 0$ (left) and $D < 0$ (right). The black double-sided arrows show the transitions from the ground m_S state which decrease in field as the applied frequency is increased.

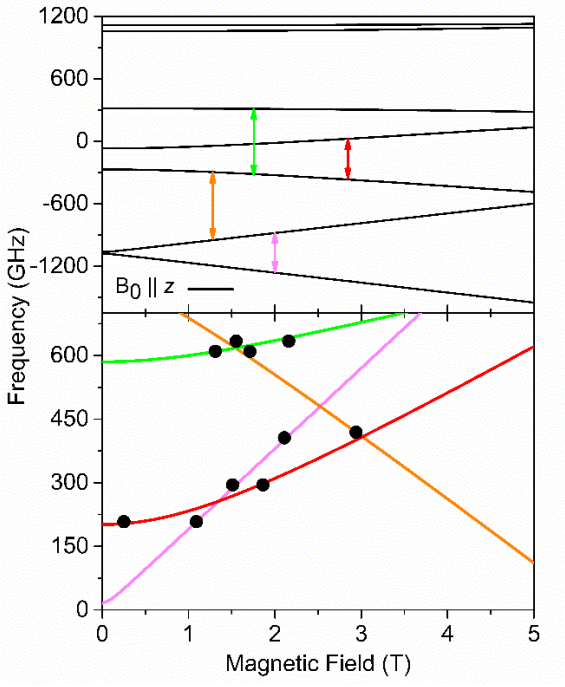

Figure S8: Zeeman diagram for B_0 parallel to the z component of the anisotropy axis using the spin Hamiltonian parameters in the text. The colored arrows correspond to the assignment of the peak indicated by the same color in Figure S6 (Top). The bottom set of axes show the frequency dependence of the transitions with the same color coding as in the top panel. The solid black circles represent the experimentally observed frequency/resonant position combinations.

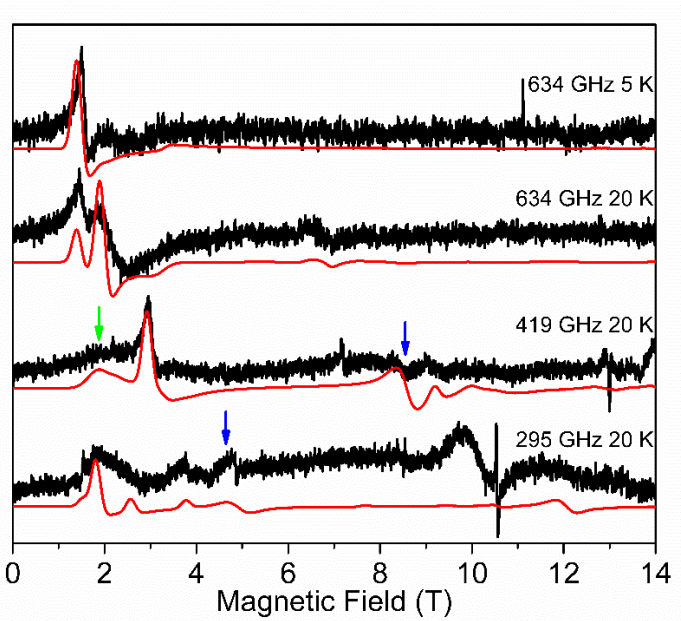

Figure S9: Experimental HFEPR spectra (black traces) and simulations (red traces) generated using the spin Hamiltonian parameters described in the text. The green and blue arrows indicate transitions which were used to determine g_x and g_y respectively.

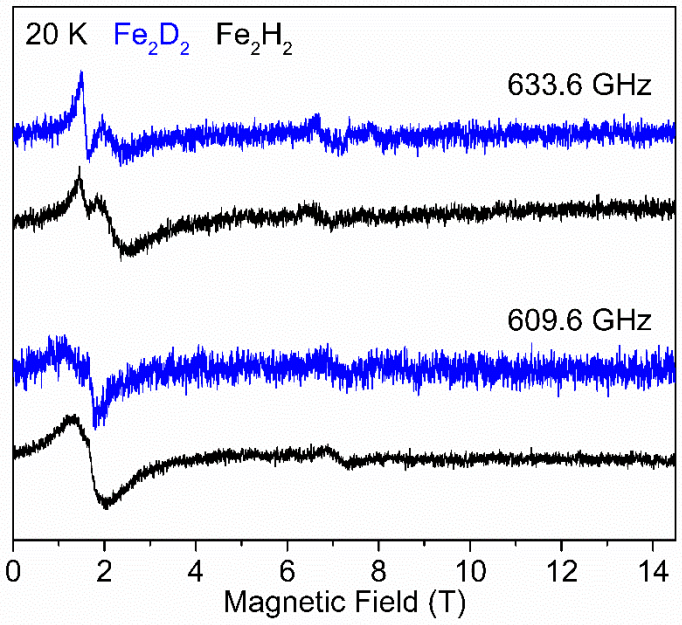

Figure S10: Comparison of HFEPR spectra between two isotopolog samples of $[Ph_2B(^tBuIm)_2Fe^{1,2}H]_2$. The black trace is for the di-protide (natural abundance) isotopolog and the blue trace is for the di-deuteride isotopolog.

Electronic Structure Calculations

All calculations were performed using density functional theory as implemented in the ORCA 3.0.3 computational software package.[33] Evaluation of the electronic energies (single point energy) was done with the def2-TZVP[34] basis set for Fe and all atoms bound to Fe; all other atoms were treated with the smaller def2-SVP basis set. For Mössbauer calculations, both Fe centers were given the CP(PPP) basis set, which includes additional polarization functions to better represent the electron density at the Fe centers. It is well known that geometric changes have large effects on magnetic properties,[35] therefore single point energies were taken from the experimentally determined crystal structure. Calculation of the magnetic exchange parameters, based on $H = -2J \cdot S_A \cdot S_B$, were performed under all possible coupling regimes using broken symmetry[36-38] DFT (BS-DFT) as implemented in ORCA. BP86 and B3LYP functionals were used to compare to experimental data as summarized in Table S8.

Table S8: Calculated exchange coupling constants (J, in cm^{-1}) at the def2-TZVP level of theory.

(calculation method)	J calc. with functional	
	BP86	B3LYP
J (method 1)	316.94	145.94
J (method 2)	237.03	109.45
J (method 3)	346.29	163.54
Experimental	110	

Three different equations have been proposed to properly calculate the exchange coupling constant, *J*. The first (method 1 in Table S8) was proposed by Noodleman et al.,[36] and advocates for the weak interaction limit of coupling, while the second (method 2 in Table S8) is the opposite extreme, the strong coupling regime. The third (method 3 in Table S8), proposed by Yamaguchi and co-workers is more robust and will reduce to the method 1 value for the weak limit and the method 2 value for strong coupling.[38] All three calculated *J* values are presented in Table S8 for completeness.

Calculation of the coupling constants clearly shows a dependence on the percentage of Hartree-Fock (HF) exchange included in the functional. The pure GGA functional, BP86, which has no HF exchange overestimates the coupling constant by approximately 100 to 200 cm^{-1}, depending on the method used. The addition of HF exchange into the functional (B3LYP) provides values that are more consistent with the experimentally determined exchange coupling constant of 110 cm^{-1}.

The Yamaguchi equation[38] can be used to pinpoint the origin of the calculated exchange coupling constant differences for BP86 and B3LYP:

$$J_{ab} = -\frac{E_{HS} - E_{BS}}{\langle S^2 \rangle_{HS} - \langle S^2 \rangle_{BS}}$$

where E_{HS} is the energy of the high spin state, E_{BS} is the energy of the broken symmetry state, $\langle S^2 \rangle_{HS}$ is the expectation value for the $\hat{S}^2$ operator for the high spin state and $\langle S^2 \rangle_{BS}$ is the expectation value for the $\hat{S}^2$ operator for the broken symmetry spin state. For this system, the high spin ($S = 3$) state will have a septet spin multiplicity and the broken symmetry state will be a triplet ($S = 1$).

The large difference in calculated coupling constants results from the BP86 and B3LYP functionals converging to two different BS states. Comparing the overlap, S, via a corresponding orbital transformation, illustrates the differences between the two BS states (Table S9). The corresponding orbital number 245 has more overlap for BP86 than for B3LYP, suggesting that the magnetic pair are more strongly coupled for the BS state in BP86. The greater overlap leads to stronger coupling, and thus the pure GGA functional BP86 overestimates the exchange coupling constant. By contrast, this overlap is reduced for B3LYP, which weakens the coupling and decreases the coupling constant to a value that is closer to that determined experimentally. This is because functionals with increased HF exchange will better stabilize electronic states having unpaired spins. Therefore, the energy difference between the high spin state and the broken symmetry state is much larger for BP86 than for B3LYP. This larger energy difference between the HS and BS states leads to larger exchange coupling constants.

Table S9: Overlap (S) calculated for the magnetic corresponding orbitals for BP86 and B3LYP.

	S calc. with functional	
Orbital Number	BP86	B3LYP
245	0.43811	0.09453
246	0.04096	0.01022
247	0.00000	0.00000
248	0.00000	0.00000

In general, when the HS and BS states have unpaired electrons, adding HF exchange is expected to decrease the exchange coupling constant J by decreasing the energy between the two states. Pure GGA functionals like BP86 will provide larger exchange coupling constants when both states have unpaired electrons. Clearly, for this system, inclusion of HF exchange is vital to correctly describing the electronic structure of the BS state that is required for calculating the exchange coupling constants.

Mössbauer calculations were also performed with both BP86 and B3LYP functionals. In this case, the differences in the isomer shift δ and the quadrupolar splitting ΔE_Q calculated for the two functionals is not as drastic as for the exchange coupling constants (Table S10). In general, added HF exchange shows little to no improvement over the pure GGA BP86 functional. The experimental Mössbauer data for the tetrahedral center are δ = 0.51, ΔE_Q = 1.92 mm/s and for the square planar center: δ = 0.35, ΔE_Q = 3.77 mm/s.

Table S10: Mössbauer data (mm/s) calculated at the CP(PPP)/def2-TVZP/def2-SVP level of theory. The CP(PPP) basis set was used for Fe, def2-TZVP for all atoms connected to the Fe, and def2-SVP for all other atoms.

Parameter	BP86	B3LYP	Experimental
δ			
Fe (T_d)	0.372	0.382	0.51
Fe (SP)	0.151	0.191	0.35
ΔE_Q			
Fe (T_d)	-1.835	-2.149	1.92
Fe (SP)	3.889	3.451	3.77

For the tetrahedral iron center, the isomer shift is qualitatively the same for both functionals, however the δ value determined using B3LYP has a slightly larger deviation from experimental values than is typically observed. A newer linear model has been proposed for the calculation of isomer shift that may help to adjust the isomer shift value but was not pursued for this system.[39] In the case of the square planar iron center, both functionals have similar errors. Despite these differences, it is important to note that both functionals predict the experimentally observed trends for the isomer shift and quadrupolar splitting values

Molecular Orbital Analysis

As described in the main text, the orbital diagram for the C_{2v} L_2Fe_2 fragment was constructed from two orthogonal L_2Fe fragments (Figure S11). In addition to the simplifications and assumptions discussed in the manuscript, for the sake of clarity, we have also assumed that orbital energies of the two iron fragments will be the same. In reality, this is not the case because the iron ligand bond lengths in for square planar site are shorter than those for the tetrahedral site.

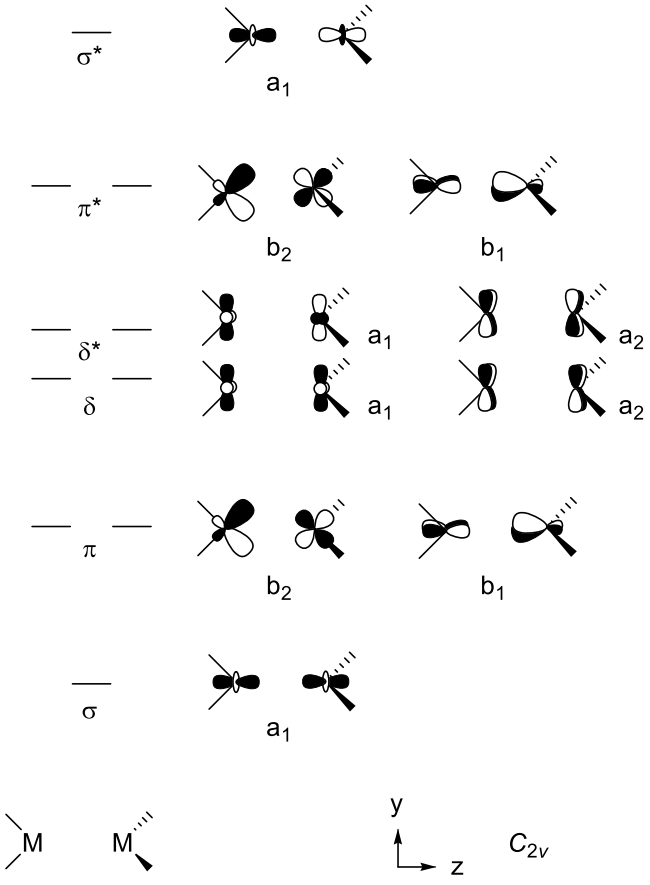

Figure S11. MO diagram for C_{2v} L_2Fe_2 fragment, including orbital representations.

As described in the main text, the frontier orbitals of $[Ph_2B(^tBuIm)_2FeH]_2$ determined by DFT computations have σ, π, and δ character with respect to the Fe···Fe interaction (Figure S12), however the low symmetry allows for orbital mixing that makes direct correspondence with the qualitative approach difficult. This orbital mixing has also hindered efforts to use multireference calculations.

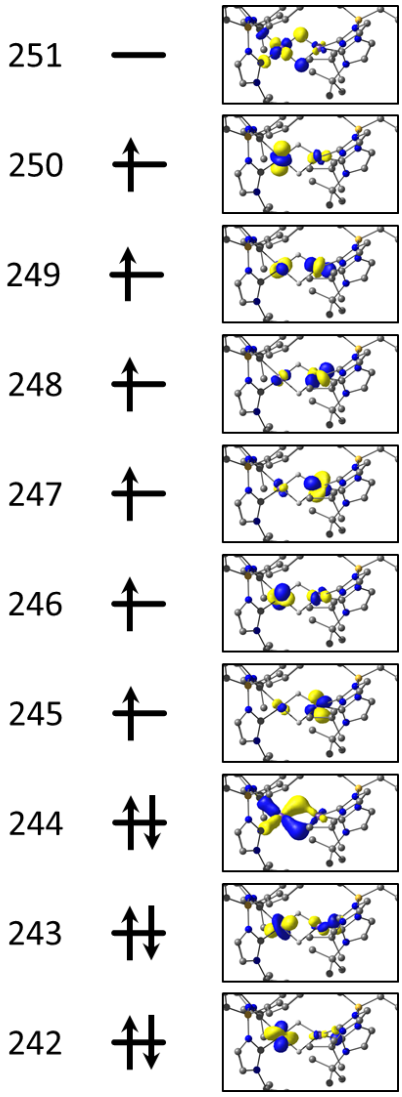

Figure S12. Unrestricted natural orbitals (UNOs) calculated for $[Ph_2B(^tBuIm)_2FeH]_2$. Orbital numbers shown.

The magnetic properties of $[Ph_2B(^tBuIm)_2FeH]_2$ are to be contrasted with those of $L_2Fe_2H_2$ complexes with approximate D_{2h} symmetry. While a number of these complexes have been reported, the ground spin states of these complexes appear to be unknown, although room temperature solution magnetic moment data suggest antiferromagnetic coupling.[16,18,40] This antiferromagnetic coupling can also be rationalized by a qualitative MO diagram. As with $[Ph_2B(^tBuIm)_2FeH]_2$, a $L_2Fe\cdots FeL_2$ fragment is constructed from two L_2Fe fragments that are aligned along the *z*-axis (Figure S13). Here, the two L_2Fe fragments are coplanar. The resulting $L_2Fe\cdots FeL_2$ unit also has orbitals with σ, π, and δ symmetry, however the two π orbitals are not degenerate: the π orbital formed from the $d_{yx}p_y$ hybrids will be better stabilized than that formed from the d_{xz} orbital due to better orbital overlap. The corresponding π* orbitals will therefore also be non-degenerate.

The full MO diagram is generated by combining the $L_2Fe\cdots FeL_2$ fragment with an orthogonal 2H unit (Figure S14). Here, the Fe-Fe σ bonding orbital (a_g) is best suited for interaction with the a_g H 1s combination, while the π_{xz} (b_{3u}) orbital has the best interaction with the b_{3u} H 1s combination. As with $[Ph_2B(^tBuIm)_2FeH]_2$, additional orbital mixing has been ignored in the interest of clarity. Due to greater orbital overlap, we suggest that the π* (b_{3u}) is sufficiently destabilized to favor spin pairing and a singlet ground state. Additional destabilization of this orbital by mixing with the δ* b_{3u} orbital is also possible.

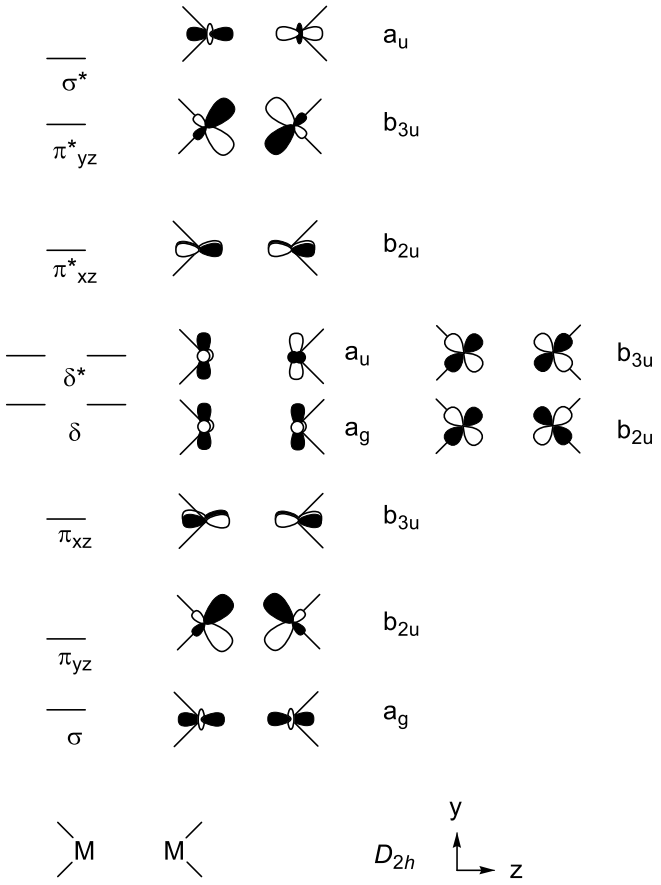

Figure S13. Fragment orbitals for the L_2Fe_2 unit in D_{2h} symmetry.

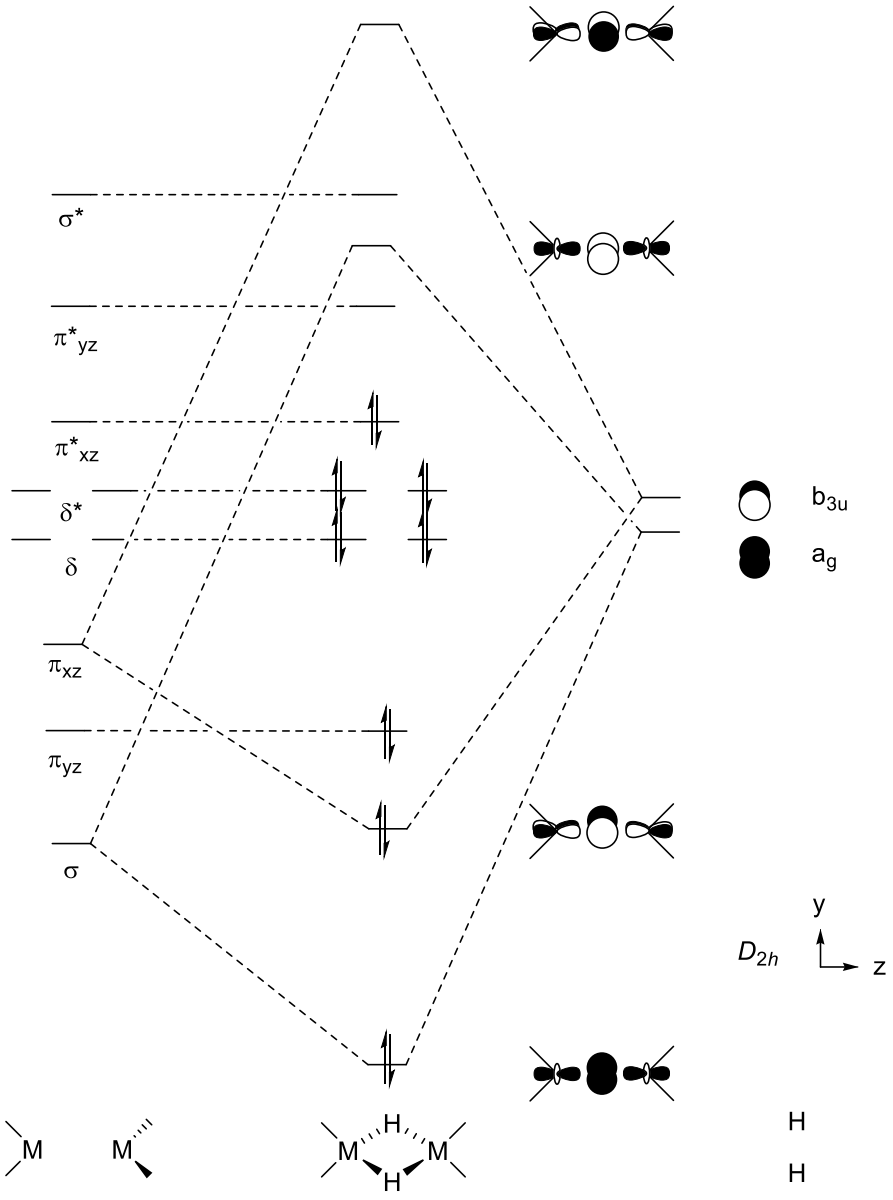

Figure S14. Fragment of orbitals for the L_2Fe_2 unit in D_{2h} symmetry.

X-ray Crystallography

Empirical formula	C52 H66 B2 Fe2 N8	
Formula weight	936.45	
Crystal color, shape, size	green plate, 0.27 × 0.25 × 0.07 mm^3	
Temperature	150(2) K	
Wavelength	0.71073 Å	
Crystal system, space group	Triclinic, P-1	
Unit cell dimensions	a = 10.8558(4) Å	α = 72.7024(18)°.
	b = 13.0976(5) Å	β = 89.0943(18)°.
	c = 19.9752(7) Å	γ = 68.2116(17)°.
Volume	2503.64(16) $Å^3$	
Z	2	
Density (calculated)	1.242 Mg/m^3	
Absorption coefficient	0.622 mm^{-1}	
F(000)	992	

Data collection	
Diffractometer	APEX II Kappa Duo, Bruker
Theta range for data collection	1.75 to 27.55°.
Index ranges	$-12 \le h \le 14$, $-17 \le k \le 16$, $-25 \le l \le 25$
Reflections collected	38636
Independent reflections	11455 [R(int) = 0.0523]
Observed Reflections	8126
Completeness to theta = 27.55°	99.2 %

Solution and Refinement	
Absorption correction	Semi-empirical from equivalents
Max. and min. transmission	0.9577 and 0.8500
Solution	Intrinsic methods
Refinement method	Full-matrix least-squares on F^2
Weighting scheme	$w = [\sigma^2 Fo^2 + AP^2 + BP]^{-1}$, with
	$P = (Fo^2 + 2\,Fc^2)/3$, A = 0.0366, B = 0.2311
Data / restraints / parameters	11455 / 0 / 597
Goodness-of-fit on F^2	1.035
Final R indices [I>2sigma(I)]	R1 = 0.0412, wR2 = 0.0857
R indices (all data)	R1 = 0.0713, wR2 = 0.0942
Largest diff. peak and hole	0.340 and –0.411 e.$Å^{-3}$

Table S11. Edited Ligfield output for square planar (S = 1) Fe(2) site.

These matrices were generated from the following terms: 5D 3P1 3P2 3D 3F1 3F2 3G 3H 1S1 1S2 1D1 1D2 1F 1G1 1G2 1I of d6 in SLMSML-basis.
One electron parametrization was taken from: AOM. The AOM-parametrization were based on the following premisses: Maximum lambda (σ, π, δ, ϕ) value included: σ. The AOM-matrices were not barycentered.

Ligator	Theta	Phi	Psi	Linear
C	90.000000	136.430000	0.000000	Yes
C'	90.000000	223.570000	0.000000	Yes
H	90.000000	42.440000	0.000000	Yes
H'	90.000000	-42.440000	0.000000	Yes

Parameter:	Value: (cm^{-1})
eσ(C)	6550.00000000
eσ(C')	6550.00000000
eσ(H)	5900.00000000
eσ(H')	5900.00000000
Racah *B*	700.00000000
Racah *C*	3100.00000000
Spin-orbit coupling (ζ)	500.00000000

Eigenvalues (in cm^{-1}) and eigenfunction labelling

Function: 1 ; Energy: 0.00000000
Spin labels: (2S+1)= 3.42151
Symmetry of eigenfunction: A1(D2*) A1(C2*)

z2	yz	xz	xy	x2-y2
0.982339	1.083510	1.901546	0.292500	1.740105

this triplet ground state d orbital occupancy corresponds roughly to: $d_{x2-y2}^2\ d_{xz}^2\ d_{yz}^1\ d_{z2}^1\ d_{xy}^0$

Function: 2 ; Energy: 1.38419161
Spin labels: (2S+1)= 3.66758
Symmetry of eigenfunction: B1(D2*) A1(C2*)

z2	yz	xz	xy	x2-y2
1.023139	1.237170	1.748155	0.365154	1.626382

similar to the above

Function: 111 ; Energy: 57.78776185
Spin labels: (2S+1)= 3.66005
Symmetry of eigenfunction: B2(D2*) B1(C2*)

z2	yz	xz	xy	x2-y2
1.031236	1.034137	1.919240	0.360204	1.655184

similar to the above – Functions 1 and 2 correspond roughly to the $m_S = \pm 1$ states; Function 111 to $m_S = 0$, comprising a spin triplet.

Function: 3 ; Energy: 304.19294837
Spin labels: (2S+1)= 3.88596
Symmetry of eigenfunction: A1(D2*) A1(C2*)

z2	yz	xz	xy	x2-y2
0.940837	1.861203	1.110591	0.535808	1.551561

Function: 112 ; Energy: 367.83549333
Spin labels: (2S+1)= 4.15670
Symmetry of eigenfunction: B3(D2*) B1(C2*)

z2	yz	xz	xy	x2-y2
1.007055	1.962117	1.033967	0.598797	1.398065

Function: 113 ; Energy: 456.58932190
Spin labels: (2S+1)= 4.97532
Symmetry of eigenfunction: B3(D2*) B1(C2*)

z2	yz	xz	xy	x2-y2
1.005983	1.408983	1.279638	0.990553	1.314843

Function: 114 ; Energy: 484.78557144
Spin labels: (2S+1)= 4.98387
Symmetry of eigenfunction: B2(D2*) B1(C2*)

z2	yz	xz	xy	x2-y2
1.002029	1.349152	1.420455	0.993940	1.234423

Function: 4 ; Energy: 527.32627346
Spin labels: (2S+1)= 4.12032
Symmetry of eigenfunction: B1(D2*) A1(C2*)

| z2 | yz | xz | xy | x2-y2 |
| 1.005401| 1.596765| 1.142132| 0.582370| 1.673332|
Function: 5 ; Energy: 594.14636335
Spin labels: (2S+1)= 4.56419
Symmetry of eigenfunction: A1(D2*) A1(C2*)
| z2 | yz | xz | xy | x2-y2 |
| 1.000324| 1.256579| 1.075980| 0.806174| 1.860943|
Function: 6 ; Energy: 723.96162428
Spin labels: (2S+1)= 4.94969
Symmetry of eigenfunction: A1(D2*) A1(C2*)
| z2 | yz | xz | xy | x2-y2 |
| 1.003160| 1.121806| 1.318561| 0.980400| 1.576073|
Function: 7 ; Energy: 739.40342966
Spin labels: (2S+1)= 4.96981
Symmetry of eigenfunction: B1(D2*) A1(C2*)
| z2 | yz | xz | xy | x2-y2 |
| 1.008613| 1.273896| 1.176689| 0.987125| 1.553676|
Function: 115 ; Energy: 812.99596793
Spin labels: (2S+1)= 4.76483
Symmetry of eigenfunction: B3(D2*) B1(C2*)
| z2 | yz | xz | xy | x2-y2 |
| 1.007636| 1.253141| 1.259331| 0.890943| 1.588948|
Function: 116 ; Energy: 816.69371585
Spin labels: (2S+1)= 4.90639
Symmetry of eigenfunction: B2(D2*) B1(C2*)
| z2 | yz | xz | xy | x2-y2 |
| 1.004226| 1.134572| 1.402737| 0.957346| 1.501118|
Function: 117 ; Energy: 1077.14761187
Spin labels: (2S+1)= 4.97721
Symmetry of eigenfunction: B2(D2*) B1(C2*)
| z2 | yz | xz | xy | x2-y2 |
| 1.001042| 1.483995| 1.513691| 0.992712| 1.008559|
Function: 118 ; Energy: 1087.57000031
Spin labels: (2S+1)= 4.99274
Symmetry of eigenfunction: B3(D2*) B1(C2*)
| z2 | yz | xz | xy | x2-y2 |
| 0.998858| 1.536260| 1.450375| 0.999671| 1.014836|
Function: 8 ; Energy: 1100.26176613
Spin labels: (2S+1)= 4.28758
Symmetry of eigenfunction: B1(D2*) A1(C2*)
| z2 | yz | xz | xy | x2-y2 |
| 1.010261| 1.272156| 1.709537| 0.663679| 1.344367|
Function: 9 ; Energy: 1284.77748532
Spin labels: (2S+1)= 4.31634
Symmetry of eigenfunction: A1(D2*) A1(C2*)
| z2 | yz | xz | xy | x2-y2 |
| 0.933191| 1.102757| 1.654855| 0.763836| 1.545362|
Function: 119 ; Energy: 1416.72745492
Spin labels: (2S+1)= 4.43632
Symmetry of eigenfunction: B2(D2*) B1(C2*)
| z2 | yz | xz | xy | x2-y2 |
| 1.023703| 1.031505| 1.699461| 0.732690| 1.512640|
Function: 10 ; Energy: 1455.33438625
Spin labels: (2S+1)= 4.06939
Symmetry of eigenfunction: A1(D2*) A1(C2*)
| z2 | yz | xz | xy | x2-y2 |
| 0.895675| 1.668319| 1.149080| 0.668966| 1.617960|

Function: 120 ; Energy: 1669.14400761
Spin labels: (2S+1)= 4.07231
Symmetry of eigenfunction: B3(D2*) B1(C2*)
| z2 | yz | xz | xy | x2-y2 |
| 1.009625| 1.790338| 1.015978| 0.561104| 1.622955|
Function: 11 ; Energy: 1738.12479426
Spin labels: (2S+1)= 3.92840
Symmetry of eigenfunction: B1(D2*) A1(C2*)
| z2 | yz | xz | xy | x2-y2 |
| 1.015047| 1.606175| 1.218683| 0.490433| 1.669662|
Function: 12 ; Energy: 2487.86507833
Spin labels: (2S+1)= 1.78110
Symmetry of eigenfunction: A1(D2*) A1(C2*)
| z2 | yz | xz | xy | x2-y2 |
| 0.415231| 1.839128| 1.736281| 0.077952| 1.931408|
Function: 121 ; Energy: 4449.98640421
Spin labels: (2S+1)= 3.00255
Symmetry of eigenfunction: B3(D2*) B1(C2*)
| z2 | yz | xz | xy | x2-y2 |
| 1.000968| 1.902647| 1.900639| 0.113909| 1.081836|
Function: 122 ; Energy: 4459.79983568
Spin labels: (2S+1)= 3.00675
Symmetry of eigenfunction: B2(D2*) B1(C2*)
| z2 | yz | xz | xy | x2-y2 |
| 1.000519| 1.901914| 1.904407| 0.113777| 1.079382|
Function: 13 ; Energy: 4487.96173672
Spin labels: (2S+1)= 3.01279
Symmetry of eigenfunction: B1(D2*) A1(C2*)
| z2 | yz | xz | xy | x2-y2 |
| 1.001059| 1.905296| 1.904747| 0.111371| 1.077527|
Function: 123 ; Energy: 6480.56324261
Spin labels: (2S+1)= 3.49136
Symmetry of eigenfunction: B3(D2*) B1(C2*)
| z2 | yz | xz | xy | x2-y2 |
| 1.901150| 1.010953| 1.046885| 0.339257| 1.701755|
Function: 124 ; Energy: 6495.49294703
Spin labels: (2S+1)= 3.54305
Symmetry of eigenfunction: B2(D2*) B1(C2*)
| z2 | yz | xz | xy | x2-y2 |
| 1.916836| 1.034341| 1.007906| 0.350466| 1.690451|
Function: 14 ; Energy: 6502.91134124
Spin labels: (2S+1)= 3.74938
Symmetry of eigenfunction: A1(D2*) A1(C2*)
| z2 | yz | xz | xy | x2-y2 |
| 1.949409| 1.006505| 1.005351| 0.415640| 1.623095|
Function: 15 ; Energy: 7165.51722946
Spin labels: (2S+1)= 4.98874
Symmetry of eigenfunction: A1(D2*) A1(C2*)
| z2 | yz | xz | xy | x2-y2 |
| 1.981033| 1.003054| 1.003553| 0.997975| 1.014385|
Function: 16 ; Energy: 7165.92117451
Spin labels: (2S+1)= 4.98910
Symmetry of eigenfunction: B1(D2*) A1(C2*)
| z2 | yz | xz | xy | x2-y2 |
| 1.981095| 1.002972| 1.003476| 0.998078| 1.014379|

Function: 125 ; Energy: 7480.43269793
Spin labels: (2S+1)= 4.18810
Symmetry of eigenfunction: B3(D2*) B1(C2*)
| z2 | yz | xz | xy | x2-y2 |
| 1.878422| 1.010287| 1.086487| 0.709212| 1.315591|
Function: 126 ; Energy: 7504.52700799
Spin labels: (2S+1)= 4.25566
Symmetry of eigenfunction: B2(D2*) B1(C2*)
| z2 | yz | xz | xy | x2-y2 |
| 1.912188| 1.052677| 1.008181| 0.706998| 1.319955|
Function: 17 ; Energy: 7648.63496803
Spin labels: (2S+1)= 4.24162
Symmetry of eigenfunction: A1(D2*) A1(C2*)
| z2 | yz | xz | xy | x2-y2 |
| 1.962408| 1.004043| 1.003698| 0.650049| 1.379802|
Function: 127 ; Energy: 8313.32034411
Spin labels: (2S+1)= 1.35017
Symmetry of eigenfunction: B3(D2*) B1(C2*)
| z2 | yz | xz | xy | x2-y2 |
| 1.101941| 1.055273| 1.798516| 0.100497| 1.943774|
Function: 128 ; Energy: 8521.24049323
Spin labels: (2S+1)= 1.22168
Symmetry of eigenfunction: B2(D2*) B1(C2*)
| z2 | yz | xz | xy | x2-y2 |
| 1.041359| 1.845543| 1.055900| 0.090654| 1.966544|
Function: 18 ; Energy: 11907.85815259
Spin labels: (2S+1)= 2.99693
Symmetry of eigenfunction: A1(D2*) A1(C2*)
| z2 | yz | xz | xy | x2-y2 |
| 0.107080| 1.893803| 1.933384| 1.004687| 1.061047|
Function: 129 ; Energy: 11938.97756007
Spin labels: (2S+1)= 3.00277
Symmetry of eigenfunction: B3(D2*) B1(C2*)
| z2 | yz | xz | xy | x2-y2 |
| 0.099460| 1.901715| 1.945627| 1.009126| 1.044072|
Function: 130 ; Energy: 11975.49622061
Spin labels: (2S+1)= 3.00289
Symmetry of eigenfunction: B2(D2*) B1(C2*)
| z2 | yz | xz | xy | x2-y2 |
| 0.088765| 1.944246| 1.937611| 1.010414| 1.018964|
Function: 19 ; Energy: 13157.06869326
Spin labels: (2S+1)= 2.98940
Symmetry of eigenfunction: B1(D2*) A1(C2*)
| z2 | yz | xz | xy | x2-y2 |
| 0.373255| 1.033486| 1.932596| 0.994114| 1.666549|
Function: 20 ; Energy: 13282.37225505
Spin labels: (2S+1)= 2.98697
Symmetry of eigenfunction: A1(D2*) A1(C2*)
| z2 | yz | xz | xy | x2-y2 |
| 0.366191| 1.071998| 1.949517| 0.988342| 1.623953|
Function: 131 ; Energy: 13300.39842281
Spin labels: (2S+1)= 2.99294
Symmetry of eigenfunction: B3(D2*) B1(C2*)
| z2 | yz | xz | xy | x2-y2 |
| 0.369620| 1.050438| 1.952112| 0.991357| 1.636473|

Function: 21 ; Energy: 13903.99100000
Spin labels: (2S+1)= 2.59094
Symmetry of eigenfunction: A1(D2*) A1(C2*)
| z2 | yz | xz | xy | x2-y2 |
| 1.580201| 1.616253| 1.380954| 0.320054| 1.102537|
Function: 22 ; Energy: 14086.31190858
Spin labels: (2S+1)= 2.95247
Symmetry of eigenfunction: B1(D2*) A1(C2*)
| z2 | yz | xz | xy | x2-y2 |
| 1.646331| 1.627805| 1.290098| 0.378558| 1.057208|
Function: 132 ; Energy: 14150.44982803
Spin labels: (2S+1)= 3.00054
Symmetry of eigenfunction: B3(D2*) B1(C2*)
| z2 | yz | xz | xy | x2-y2 |
| 1.646622| 1.653179| 1.284777| 0.385637| 1.029785|
Function: 23 ; Energy: 14197.94150851
Spin labels: (2S+1)= 2.92389
Symmetry of eigenfunction: A1(D2*) A1(C2*)
| z2 | yz | xz | xy | x2-y2 |
| 1.512014| 1.439943| 1.527003| 0.414940| 1.106101|
Function: 24 ; Energy: 14312.27375467
Spin labels: (2S+1)= 2.92967
Symmetry of eigenfunction: B1(D2*) A1(C2*)
| z2 | yz | xz | xy | x2-y2 |
| 1.457341| 1.382630| 1.538515| 0.465077| 1.156436|
Function: 133 ; Energy: 14337.27716871
Spin labels: (2S+1)= 3.00112
Symmetry of eigenfunction: B2(D2*) B1(C2*)
| z2 | yz | xz | xy | x2-y2 |
| 1.291856| 1.465859| 1.510616| 0.530896| 1.200773|
Function: 25 ; Energy: 14431.84781289
Spin labels: (2S+1)= 2.97399
Symmetry of eigenfunction: B1(D2*) A1(C2*)
| z2 | yz | xz | xy | x2-y2 |
| 0.489851| 1.859733| 1.064879| 0.952122| 1.633415|
Function: 26 ; Energy: 14485.60726136
Spin labels: (2S+1)= 2.98479
Symmetry of eigenfunction: A1(D2*) A1(C2*)
| z2 | yz | xz | xy | x2-y2 |
| 0.485661| 1.874451| 1.055851| 0.952772| 1.631265|
Function: 134 ; Energy: 14490.14555651
Spin labels: (2S+1)= 2.99416
Symmetry of eigenfunction: B2(D2*) B1(C2*)
| z2 | yz | xz | xy | x2-y2 |
| 0.639419| 1.804105| 1.112659| 0.892116| 1.551701|
Function: 27 ; Energy: 15305.03117760
Spin labels: (2S+1)= 1.16424
Symmetry of eigenfunction: B1(D2*) A1(C2*)
| z2 | yz | xz | xy | x2-y2 |
| 1.869296| 1.047770| 1.040244| 0.149647| 1.893043|
Function: 28 ; Energy: 15395.63072072
Spin labels: (2S+1)= 1.53992
Symmetry of eigenfunction: A1(D2*) A1(C2*)
| z2 | yz | xz | xy | x2-y2 |
| 1.256218| 1.647229| 1.640020| 0.221548| 1.234986|

Function: 29 ; Energy: 16692.61490438
Spin labels: (2S+1)= 1.07604
Symmetry of eigenfunction: A1(D2*) A1(C2*)
| z2 | yz | xz | xy | x2-y2 |
| 1.615069| 1.150305| 1.190008| 0.255428| 1.789190|
Function: 30 ; Energy: 17496.97480384
Spin labels: (2S+1)= 2.98285
Symmetry of eigenfunction: B1(D2*) A1(C2*)
| z2 | yz | xz | xy | x2-y2 |
| 1.044213| 1.107438| 1.313893| 0.979323| 1.555133|
Function: 135 ; Energy: 17516.56079050
Spin labels: (2S+1)= 2.99797
Symmetry of eigenfunction: B3(D2*) B1(C2*)
| z2 | yz | xz | xy | x2-y2 |
| 1.049147| 1.019316| 1.250937| 0.991167| 1.689433|
Function: 136 ; Energy: 17550.94295643
Spin labels: (2S+1)= 2.99877
Symmetry of eigenfunction: B2(D2*) B1(C2*)
| z2 | yz | xz | xy | x2-y2 |
| 1.044030| 1.153613| 1.027100| 0.987376| 1.787881|
Function: 31 ; Energy: 17598.44920010
Spin labels: (2S+1)= 2.63097
Symmetry of eigenfunction: B1(D2*) A1(C2*)
| z2 | yz | xz | xy | x2-y2 |
| 0.846813| 1.496210| 1.565412| 1.002370| 1.089195|
Function: 32 ; Energy: 17795.72762619
Spin labels: (2S+1)= 2.98755
Symmetry of eigenfunction: A1(D2*) A1(C2*)
| z2 | yz | xz | xy | x2-y2 |
| 1.044824| 1.083489| 1.880740| 0.987420| 1.003528|
Function: 137 ; Energy: 17870.18567385
Spin labels: (2S+1)= 2.99841
Symmetry of eigenfunction: B3(D2*) B1(C2*)
| z2 | yz | xz | xy | x2-y2 |
| 1.049108| 1.050363| 1.666589| 0.999789| 1.234151|
Function: 33 ; Energy: 18049.36679014
Spin labels: (2S+1)= 3.01046
Symmetry of eigenfunction: A1(D2*) A1(C2*)
| z2 | yz | xz | xy | x2-y2 |
| 1.007077| 1.836830| 1.099066| 1.006725| 1.050303|
Function: 34 ; Energy: 18052.58333962
Spin labels: (2S+1)= 2.95065
Symmetry of eigenfunction: B1(D2*) A1(C2*)
| z2 | yz | xz | xy | x2-y2 |
| 1.031654| 1.432097| 1.259834| 0.979945| 1.296470|
Function: 138 ; Energy: 18109.29725947
Spin labels: (2S+1)= 3.01253
Symmetry of eigenfunction: B2(D2*) B1(C2*)
| z2 | yz | xz | xy | x2-y2 |
| 1.028507| 1.703155| 1.080973| 1.000609| 1.186755|
Function: 35 ; Energy: 18313.59063506
Spin labels: (2S+1)= 2.97043
Symmetry of eigenfunction: A1(D2*) A1(C2*)
| z2 | yz | xz | xy | x2-y2 |
| 1.134705| 0.659689| 1.449811| 0.975325| 1.780470|

start - transitions contributing to observed Vis band

Function: 139 ; Energy: 18327.60414397
Spin labels: (2S+1)= 2.99822
Symmetry of eigenfunction: B2(D2*) B1(C2*)
| z2 | yz | xz | xy | x2-y2 |
| 1.122004| 0.611228| 1.504139| 0.989392| 1.773237|
Function: 140 ; Energy: 18331.08187737
Spin labels: (2S+1)= 3.00009
Symmetry of eigenfunction: B3(D2*) B1(C2*)
| z2 | yz | xz | xy | x2-y2 |
| 1.125904| 0.593598| 1.489629| 0.988684| 1.802186|
Function: 36 ; Energy: 19040.02193280
Spin labels: (2S+1)= 1.53320
Symmetry of eigenfunction: B1(D2*) A1(C2*)
| z2 | yz | xz | xy | x2-y2 |
| 0.298002| 1.865639| 1.795863| 1.019121| 1.021374|
Function: 141 ; Energy: 19324.26041913
Spin labels: (2S+1)= 4.50687
Symmetry of eigenfunction: B3(D2*) B1(C2*)
| z2 | yz | xz | xy | x2-y2 |
| 1.025340| 1.038623| 1.010955| 1.757715| 1.167368|
Function: 37 ; Energy: 19327.03304947
Spin labels: (2S+1)= 4.67299
Symmetry of eigenfunction: B1(D2*) A1(C2*)
| z2 | yz | xz | xy | x2-y2 |
| 1.016068| 1.003338| 1.020120| 1.840457| 1.120017|
Function: 142 ; Energy: 19332.02349757
Spin labels: (2S+1)= 4.45709
Symmetry of eigenfunction: B2(D2*) B1(C2*)
| z2 | yz | xz | xy | x2-y2 |
| 1.028215| 1.040905| 1.014381| 1.736413| 1.180086|
Function: 38 ; Energy: 19372.89716888
Spin labels: (2S+1)= 4.84446
Symmetry of eigenfunction: B1(D2*) A1(C2*)
| z2 | yz | xz | xy | x2-y2 |
| 0.999784| 1.038349| 1.015270| 1.924790| 1.021807|
Function: 39 ; Energy: 19373.62793204
Spin labels: (2S+1)= 4.83786
Symmetry of eigenfunction: A1(D2*) A1(C2*)
| z2 | yz | xz | xy | x2-y2 |
| 1.003256| 1.033388| 1.036012| 1.921727| 1.005616|
Function: 143 ; Energy: 19401.52050924
Spin labels: (2S+1)= 3.21254
Symmetry of eigenfunction: B2(D2*) B1(C2*)
| z2 | yz | xz | xy | x2-y2 |
| 1.073994| 1.101032| 1.042355| 1.133850| 1.648769|
Function: 144 ; Energy: 19445.53356224
Spin labels: (2S+1)= 3.37067
Symmetry of eigenfunction: B3(D2*) B1(C2*)
| z2 | yz | xz | xy | x2-y2 |
| 1.068124| 1.219089| 1.031829| 1.199370| 1.481588|
Function: 40 ; Energy: 19491.38261988
Spin labels: (2S+1)= 3.24758
Symmetry of eigenfunction: B1(D2*) A1(C2*)
| z2 | yz | xz | xy | x2-y2 |
| 1.080504| 0.997556| 1.011202| 1.133903| 1.776836|

end - transitions contributing to observed Vis band

Function: 145 ; Energy: 19520.98644450
Spin labels: (2S+1)= 2.99669
Symmetry of eigenfunction: B3(D2*) B1(C2*)

z2	yz	xz	xy	x2-y2
1.075600	1.606753	1.130022	1.011910	1.175714

Function: 146 ; Energy: 19523.80074162
Spin labels: (2S+1)= 3.15969
Symmetry of eigenfunction: B2(D2*) B1(C2*)

z2	yz	xz	xy	x2-y2
1.074538	1.746100	1.076779	1.088814	1.013769

Function: 41 ; Energy: 19550.15046502
Spin labels: (2S+1)= 2.98742
Symmetry of eigenfunction: A1(D2*) A1(C2*)

z2	yz	xz	xy	x2-y2
1.083867	1.804573	1.169495	1.006030	0.936035

Function: 42 ; Energy: 20008.52381997
Spin labels: (2S+1)= 1.69913
Symmetry of eigenfunction: A1(D2*) A1(C2*)

z2	yz	xz	xy	x2-y2
1.456955	1.267922	1.037747	0.564126	1.673250

Function: 147 ; Energy: 20124.21858356
Spin labels: (2S+1)= 3.00118
Symmetry of eigenfunction: B2(D2*) B1(C2*)

z2	yz	xz	xy	x2-y2
1.031112	1.670012	1.077245	0.969647	1.251984

Function: 43 ; Energy: 20149.43061127
Spin labels: (2S+1)= 3.00453
Symmetry of eigenfunction: B1(D2*) A1(C2*)

z2	yz	xz	xy	x2-y2
1.044400	1.657249	1.084459	0.968963	1.244928

Function: 44 ; Energy: 20253.52386160
Spin labels: (2S+1)= 2.42881
Symmetry of eigenfunction: A1(D2*) A1(C2*)

z2	yz	xz	xy	x2-y2
1.220669	1.514087	1.088398	0.769950	1.406896

Function: 148 ; Energy: 20645.50822528
Spin labels: (2S+1)= 3.00622
Symmetry of eigenfunction: B3(D2*) B1(C2*)

z2	yz	xz	xy	x2-y2
1.008066	1.074239	1.679574	0.959998	1.278122

Function: 45 ; Energy: 20687.96999142
Spin labels: (2S+1)= 3.00781
Symmetry of eigenfunction: B1(D2*) A1(C2*)

z2	yz	xz	xy	x2-y2
0.995988	1.076907	1.684987	0.963801	1.278317

Function: 46 ; Energy: 20710.96768223
Spin labels: (2S+1)= 2.95626
Symmetry of eigenfunction: A1(D2*) A1(C2*)

z2	yz	xz	xy	x2-y2
1.019397	1.084232	1.676610	0.937435	1.282326

Function: 149 ; Energy: 21642.97092642
Spin labels: (2S+1)= 1.14851
Symmetry of eigenfunction: B2(D2*) B1(C2*)

z2	yz	xz	xy	x2-y2
1.025240	1.275352	1.528028	0.762851	1.408529

Function: 150 ; Energy: 21991.14415290
Spin labels: (2S+1)= 2.63852
Symmetry of eigenfunction: B3(D2*) B1(C2*)

z2	yz	xz	xy	x2-y2
1.195387	1.148467	1.695853	0.930374	1.029919

Function: 47 ; Energy: 22059.04892278
Spin labels: (2S+1)= 3.02912
Symmetry of eigenfunction: B1(D2*) A1(C2*)

z2	yz	xz	xy	x2-y2
1.104131	1.194256	1.693130	1.034842	0.973641

Function: 48 ; Energy: 22092.95685495
Spin labels: (2S+1)= 3.01524
Symmetry of eigenfunction: A1(D2*) A1(C2*)

z2	yz	xz	xy	x2-y2
1.093392	1.197552	1.712184	1.030412	0.966460

Function: 151 ; Energy: 22399.93397100
Spin labels: (2S+1)= 1.85801
Symmetry of eigenfunction: B3(D2*) B1(C2*)

z2	yz	xz	xy	x2-y2
1.146047	1.287252	1.379595	0.802249	1.384857

Function: 152 ; Energy: 22432.29513440
Spin labels: (2S+1)= 2.90537
Symmetry of eigenfunction: B2(D2*) B1(C2*)

z2	yz	xz	xy	x2-y2
1.105945	1.578363	1.188330	1.010870	1.116493

Function: 49 ; Energy: 22530.39709313
Spin labels: (2S+1)= 3.04697
Symmetry of eigenfunction: B1(D2*) A1(C2*)

z2	yz	xz	xy	x2-y2
1.077903	1.561815	1.213410	1.043530	1.103342

Function: 50 ; Energy: 22572.93556753
Spin labels: (2S+1)= 3.03450
Symmetry of eigenfunction: A1(D2*) A1(C2*)

z2	yz	xz	xy	x2-y2
1.053468	1.672177	1.233532	1.040882	0.999940

Function: 153 ; Energy: 22777.08352188
Spin labels: (2S+1)= 2.59044
Symmetry of eigenfunction: B3(D2*) B1(C2*)

z2	yz	xz	xy	x2-y2
1.241033	1.055676	1.158746	0.913835	1.630710

Function: 154 ; Energy: 22784.17938108
Spin labels: (2S+1)= 2.90104
Symmetry of eigenfunction: B2(D2*) B1(C2*)

z2	yz	xz	xy	x2-y2
1.178433	1.191016	1.068821	0.984940	1.576790

Function: 51 ; Energy: 22787.76064538
Spin labels: (2S+1)= 3.02515
Symmetry of eigenfunction: B1(D2*) A1(C2*)

z2	yz	xz	xy	x2-y2
1.154725	1.119889	1.060009	1.023792	1.641584

Function: 155 ; Energy: 23534.39173584
Spin labels: (2S+1)= 1.45559
Symmetry of eigenfunction: B2(D2*) B1(C2*)

z2	yz	xz	xy	x2-y2
1.307245	1.293938	1.445538	0.749401	1.203878

Function: 156 ; Energy: 23657.96502041
Spin labels: (2S+1)= 1.65363
Symmetry of eigenfunction: B3(D2*) B1(C2*)
| z2 | yz | xz | xy | x2-y2 |
| 1.293930| 1.532984| 1.126460| 0.899431| 1.147194|
Function: 52 ; Energy: 24231.71786093
Spin labels: (2S+1)= 3.00033
Symmetry of eigenfunction: B1(D2*) A1(C2*)
| z2 | yz | xz | xy | x2-y2 |
| 1.803606| 1.015922| 1.004256| 1.010739| 1.165476|
Function: 157 ; Energy: 24252.16687453
Spin labels: (2S+1)= 2.80944
Symmetry of eigenfunction: B2(D2*) B1(C2*)
| z2 | yz | xz | xy | x2-y2 |
| 1.817064| 1.066907| 1.033666| 0.970184| 1.112179|
Function: 158 ; Energy: 24463.96461193
Spin labels: (2S+1)= 2.44385
Symmetry of eigenfunction: B3(D2*) B1(C2*)
| z2 | yz | xz | xy | x2-y2 |
| 1.615361| 1.222273| 1.057207| 0.956251| 1.148908|
Function: 159 ; Energy: 24814.95180789
Spin labels: (2S+1)= 2.92610
Symmetry of eigenfunction: B3(D2*) B1(C2*)
| z2 | yz | xz | xy | x2-y2 |
| 1.609118| 1.352555| 1.185920| 1.021098| 0.831308|
Function: 160 ; Energy: 24815.18257351
Spin labels: (2S+1)= 2.94040
Symmetry of eigenfunction: B2(D2*) B1(C2*)
| z2 | yz | xz | xy | x2-y2 |
| 1.630227| 1.343092| 1.142564| 1.022252| 0.861865|
Function: 53 ; Energy: 24819.97681522
Spin labels: (2S+1)= 2.98959
Symmetry of eigenfunction: A1(D2*) A1(C2*)
| z2 | yz | xz | xy | x2-y2 |
| 1.623873| 1.327529| 1.160781| 1.037771| 0.850046|
Function: 54 ; Energy: 25126.05794200
Spin labels: (2S+1)= 2.98967
Symmetry of eigenfunction: B1(D2*) A1(C2*)
| z2 | yz | xz | xy | x2-y2 |
| 1.851016| 0.949046| 0.742634| 0.978685| 1.478618|
Function: 55 ; Energy: 25162.56994332
Spin labels: (2S+1)= 2.99177
Symmetry of eigenfunction: A1(D2*) A1(C2*)
| z2 | yz | xz | xy | x2-y2 |
| 1.850574| 0.967556| 0.709436| 0.975212| 1.497221|
Function: 56 ; Energy: 25200.11930940
Spin labels: (2S+1)= 2.97062
Symmetry of eigenfunction: B1(D2*) A1(C2*)
| z2 | yz | xz | xy | x2-y2 |
| 1.858582| 0.785855| 0.902398| 0.994014| 1.459151|
Function: 161 ; Energy: 25221.68795496
Spin labels: (2S+1)= 2.99089
Symmetry of eigenfunction: B3(D2*) B1(C2*)
| z2 | yz | xz | xy | x2-y2 |
| 1.870452| 1.078568| 0.553730| 0.984832| 1.512417|

Function: 162 ; Energy: 25267.85130392
Spin labels: (2S+1)= 2.97794
Symmetry of eigenfunction: B2(D2*) B1(C2*)

z2	yz	xz	xy	x2-y2
1.849354	0.686037	1.078801	0.980051	1.405757

Function: 57 ; Energy: 25274.21074849
Spin labels: (2S+1)= 2.98726
Symmetry of eigenfunction: A1(D2*) A1(C2*)

z2	yz	xz	xy	x2-y2
1.858680	0.786494	0.919135	0.990695	1.444995

Function: 163 ; Energy: 27018.15927110
Spin labels: (2S+1)= 2.98701
Symmetry of eigenfunction: B2(D2*) B1(C2*)

z2	yz	xz	xy	x2-y2
1.832330	0.992175	1.022770	1.037422	1.115303

Function: 164 ; Energy: 27047.62900380
Spin labels: (2S+1)= 2.99483
Symmetry of eigenfunction: B3(D2*) B1(C2*)

z2	yz	xz	xy	x2-y2
1.831289	0.999859	1.010022	1.037872	1.120958

Function: 58 ; Energy: 27096.19281766
Spin labels: (2S+1)= 2.99317
Symmetry of eigenfunction: B1(D2*) A1(C2*)

z2	yz	xz	xy	x2-y2
1.829205	0.996264	1.013886	1.036658	1.123987

Function: 165 ; Energy: 27989.55409186
Spin labels: (2S+1)= 2.97479
Symmetry of eigenfunction: B3(D2*) B1(C2*)

z2	yz	xz	xy	x2-y2
1.910539	1.019055	0.987371	1.032006	1.051028

States above 28 000 cm^{-1} (λ = 357 nm) are truncated.

References

1. Hickey, A. K.; Lee, W.-T.; Chen, C.-H.; Pink, M.; Smith, J. M. *Organometallics* **2016**, *35*, 3069.

2. Baker, M. V.; Field, L. D.; Hambley, T. W. *Inorg. Chem*. **1988**, 27, 2872.

3. Prisecaru, I. WMOSS4 Mössbauer Spectral Analysis Software, www.wmoss.org, 2009-2016.

4. Hawrelak, E. J.; Bernskoetter, W. H.; Lobkovsky, E.; Yee, G. T.; Bill, E.; Chirik, P. J. *Inorg. Chem.* **2005**, *44*, 3103.

5. Liu, Y.; Luo, L.; Xiao, J.; Wang, L.; Song, Y.; Qu, J.; Luo, Y.; Deng, L. *Inorg. Chem.* **2015**, *54*, 4752.

6. Muller, G.; Sales, J.; Vinaixa, J.; Tejada, J. *Inorg. Chim. Acta* **1982**, *60*, 227.

7. Pinkert, D.; Dmeshko, S.; Schax, F.; Braun, B.; Meyer, F.; Limberg, C. *Angew. Chem*. *Int. Ed.* **2013**, *52*, 5155.

8. Pascualini, M. E.; Di Russo, N. V.; Thuijs, A. E.; Ozarowski, A.; Stoian, S. A.; Abboud, K. A.; Christou, G.; Veige, A. S. *Chem. Sci.* **2015**, *6*, 608.

9. Ouyang, Z.; Meng, Y.; Cheng, J.; Xiao, J.; Gao, S.; Deng, L. *Organometallics* **2016**, *35*, 1361

10. Gütlich, P.; Bill, E.; Trautwein, A. X. *Mössbauer Spectroscopy and Transition Metal Chemistry*, Springer: Berlin, 2011; p 441.

11. MacLeod, K. C.; Vinyard, D. J.; Holland, P. L. *J. Am. Chem. Soc.* **2014**, *136*, 10226.

12. Dugan, T. R.; Bill, E.; MacLeod, K. C.; Christian, G. J.; Cowley, R. E.; Brennessel, W. W.; Ye, S.; Neese, F.; Holland, P. L. *J. Am. Chem. Soc.* **2012**, *134*, 20352.

13. Roy, N.; Sproules, S.; Bill, E.; Weyhermüller, T.; Wieghardt, K. *Inorg. Chem.* **2008**, *47*, 10911.

14. Fang, M.; Wilson, S. R.; Suslick, K. S. *J. Am. Chem. Soc.*, **2008**, *130*, 1134.

15. Rodriguez, M. M.; Bill, E.; Brennessel, W. W.; Holland, P. L. *Science* **2011**, *334*, 780.

16. Dugan, T. R.; Bill, E.; MacLeod, K. C.; Brennessel, W. W.; Holland, P. L. *Inorg. Chem.* **2014**, *53*, 2370.

17. Dugan, T. R.; Holland, P. L. *J. Organomet. Chem.* **2009**, 694, 2825

18. Bellows, S. M.; Arnet, N. A.; Gurubasavaraj, P. M. Brennessel, W. W.; Bill, E.; Cundari, T. R.; Holland, P. L. *J. Am. Chem. Soc.* **2016**, *138*, 12112.

19. Bain, G. A.; Berry, J. F. *J. Chem. Educ.* **2008**, *85*, 532.

20. a) Trofimenko, S. *Polyhedron* **2004**, *23*, 197-203. This is part of a special issue on scorpionate ligands, of which other articles are relevant. b) Trofimenko, S. *Scorpionates: The coordination chemistry of polypyrazolylborate ligands*, London: Imperial College Press, 1999.

21. Liu, Y.; Shi, M.; Deng, L. *Organometallics* **2014**, *33*, 5660.

22. Hahn, A. W.; Van Kuiken, B. E.; al Samarai, M.; Atanasov, M.; Weyhermüller, T.; Cui, Y.-T.; Miyawaki, J.; Harada, Y.; Nicolaou, A.; DeBeer, S. *Inorg. Chem.* **2017**, *56*, 8203.

23. Gruen, D. M.; McBeth, R. L. *Pure Appl. Chem*. **1963**, *6*, 23-48. (See p 38).

24. The Racah parameters for Fe^{2+} free-ion are: $B = 897.143\ cm^{-1}$, $C = 3877.143\ cm^{-1}$ ($C/B = 4.32$), taken from: Brorson, M.; Schaeffer, C. E. *Inorg. Chem*. **1988**, *27*, 2522-2530; (see Table II).

25. Nieto, I.; Bontchev, R. P.; Ozarowski, A.; Smirnov, D.; Krzystek, J.; Telser, J.; Smith, J. M. *Inorg. Chim. Acta* **2009**, *362*, 4449.

26. Linn, D. E.; Gibbins, S. G. *Inorg. Chem.* **1997**, *36*, 3461.

27. Bau, R.; Ho, D. M.; Gibbins, S. G. *J. Am. Chem. Soc.* **1981**, *103*, 4960.

28. Bau, R.; Chiang, M. Y.; Ho, D. M.; Gibbins, S. G.; Emge, T. J.; Koetzle, T. F. *Inorg. Chem.* **1984**, *23*, 2823.

29. Scheidt, W. R.; Reed, C. A. *Chem. Rev.* **1981**, *81*, 543.

30. Pascualini, M.; Stoian, S. A.; Ozarowski, A.; Abboud, K. A.; Veige, A. S. *Inorg. Chem.* **2016**, *55*, 5191.

31. Xu, S.; Bucinsky, L.; Breza, M.; Krzystek, J.; Chen, C.-H.; Pink, M.; Telser, J.; Smith, J. M. *Inorg. Chem.* **2017**, *56*, 14315.

32. Bendix, J., Ligfield. In *Comprehensive Coordination Chemistry II, Volume 2: Fundamentals: Physical Methods, Theoretical Analysis, and Case Studies*, Lever, A. B. P., Ed. Elsevier: Amsterdam, 2003; Vol. 2, pp 673-676.

33. Neese, F. *WIREs Comput. Mol. Sci.* **2012**, *2*, 73.

34. Pantazis, D. A.; Chen, X.-Y.; Landis, C. R.; Neese, F. *J. Chem. Theory Comp.* **2008**, 4, 908.

35. Reger, D. L.; Pascui, A. E.; Smith, M. D.; Jezierska, J.; Ozarowski, A. *Inorg. Chem.* **2015**, 54, 1487.

36. (a) Ginsberg. A. P. *J. Am. Chem. Soc.* **1980**, 102, 111; (b) Noodleman, L. *J. Chem. Phys.* **1981**, 74, 5737; (c) Noodleman, L.; Davidson, E. R. *Chem. Phys.* **1985**, 109, 131.

37. Bencini, A. Gatteschi, D. *J. Am. Chem. Soc.* **1980**, 108, 5763.

38. Soda, T.; Kitagawa, Y.; Onishi T.; Takano Y.; Shigeta, Y.; Nagao, H.; Yoshioka, Y.; Yamaguchi, K. *Chem. Phys. Lett.* **2000**, 319, 223.

39. Neese, F. *Coord. Chem. Rev.* **2009**, 253, 526.

40. (a) Smith, J. M.; Lachicotte, R. J.; Holland, P. L. *J. Am. Chem. Soc.* **2003**, *125*, 15752; (b) Vela, J.; Smith, J. M.; Yu, Y.; Ketterer, N. A.; Flaschenriem, C. J.; Lachicotte, R. J.; Holland, P. L. *J. Am. Chem. Soc.* **2005**, *127*, 7857; (b) Yu, Y.; Sadique, A. R.; Smith, J. M.; Dugan, T. R.; Cowley, R. E.; Brennessel, W. W.; Flaschenriem, C. J.; Bill, E.; Cundari, T. R.; Holland, P. L. *J. Am. Chem. Soc.* **2008**, *130*, 6624; (c) Hein, N. M.; Pick, F. S.; Fryzuk, M. D. *Inorg. Chem.* **2017**, *56*, 14513.